On Vortex Breakdown in Swirling Annular Jets

Carl Fredrik Stein

NO 1998-14/ISSN 0347-2809

1998
Mathematics
Department of Mathematics
Chalmers University of Technology
and Göteborg University
S-412 96 Göteborg, Sweden

Abstract

When the degree of swirl of a swirling annular jet increases, a zone of reversed flow along the symmetry axis appears suddenly; We will term this event vortex breakdown, and despite extensive theoretical research the question of its underlying mechanisms still lacks a definite answer. The uncertainty of what governs vortex breakdown is manifested in the common use of a variety of different parameters to describe the degree of swirl. With the use of numerics it is shown that some of these are more dependent of the inflow geometry than others. Conically self-similar solutions to the Navier-Stokes equations may increase the understanding of vortex breakdown in swirling annular jets. We will prove a uniqueness and a regularity result for conically self-similar solutions and in addition we will show that the existence of a conically self-similar solution to the Navier-Stokes equations implies the existence of a second-order non-swirling correction term. We also give sufficient conditions for this second order non-swirling correction term to have a vanishing second-order contribution to the total axial momentum flux. Finally, we discuss the relevance of conically self-similar solutions to the study of swirling annular jets.

Key words : swirling jets, vortex breakdown, conical self-similarity, swirl numbers, CFD

Acknowledgements

I would like to express my gratitude to my supervisor Jöran Bergh, for his encouragement and his many helpful suggestions, which helped me improve the mathematical part of the thesis.

I am also indebted to Lars-Erik Eriksson at Volvo Aero Corporation for introducing me to swirling annular jets, and for letting me use his computer codes for turbulent axisymmetric flow, which were of tremendous use throughout the duration of the project. Further, I am obliged to Frank Holzäpfel for sending me his experimental results on swirling free jets.

I would also like to thank Lennart Löfdahl for his enthusiasm, and for the fruitful discussions we have had. On the same note, I would like to thank Matthias Holschneider for his hospitality as well as for his guidance and encouragement, which improved me considerably as a mathematician.

Part of the work was funded by the Swedish Institute of Applied Mathematics (ITM). The two months I spent at Volvo Aero Corporation were financed by the Swedish Network of Applied Mathematics (NTM) as part of their university-industry exchange programme. I am also thankful for the travel grants I received from the Adlerbert Research Foundation (Adlerbertska Forskningsfonden).

Finally, I would like to thank Christina for continuous support during the course of the project.

Contents

Preface 1

1 Introduction 3
- 1.1 Background . . . 3
- 1.2 The application of swirling jets in combustion chambers . . . 4
- 1.3 Vortex breakdown theory . . . 4
- 1.4 Conically self-similar solutions to the Navier-Stokes equations 5
- 1.5 Numerical method . . . 7
  - 1.5.1 Geometry of the test cases . . . 7
  - 1.5.2 Inlet and outlet conditions . . . 7

2 The qualitative behaviour of swirling annular jets 9

3 Towards a vortex breakdown condition independent of the inflow geometry 13
- 3.1 Introduction . . . 13
- 3.2 The different dimensionless numbers used to characterise swirl 14
- 3.3 Geometry of the test cases . . . 16
- 3.4 Results and discussion . . . 17
  - 3.4.1 The critical degree of swirl . . . 17

4 Some mathematical aspects of conically self-similar solutions to the Navier-Stokes equations 19
- 4.1 Introduction . . . 19
- 4.2 The basic model . . . 21
  - 4.2.1 Boundary conditions . . . 23
  - 4.2.2 The total axial flow force . . . 24
- 4.3 On the existence of solutions to the conically self-similar equations . . . 26
- 4.4 Regularity and uniqueness of conically self-similar solutions . 27
- 4.5 On the existence and regularity of a second order non-swirling correction term to conically self-similar solutions . . . 38
- 4.6 Numerical computation of conically self-similar solutions and the second-order non-swirling correction term . . . 41

4.6.1 The numerical method for finding conically self-similar solutions to the Navier-Stokes equations 42
4.6.2 The numerical results 42

5 On the applicability of conical self-similarity to the understanding of combustion chamber flows **49**
5.1 Introduction 49
5.2 On the existence of a region of approximately self-similar flow in combustion chambers 50
5.3 On the relation between the results of CFD simulations of combustion chambers and conically self-similar solutions to the Navier-Stokes equations 52
5.3.1 Some reasons why combustion chamber flows are *not* conically self-similar 52
5.3.2 The role of Q and L_z in conically self-similar solutions 53
5.3.3 A numerical comparison 55
5.4 On the presence of approximate conical self-similarity in swirling free jets 58

6 Summary **61**

A The incompressible Navier-Stokes equations in spherical coordinates **63**

Bibliography **64**

Preface

This licentiate thesis is written to conclude a five-semester ECMI (European Consortium in Industrial Mathematics) programme in applied mathematics. Even though both core and optional courses are part of it, the main element in the ECMI programme is the final project, which must treat a mathematical problem that emanates from industry.

This licentiate project emerged from Volvo Aero Corporation, Trollhättan, Sweden, and it concerns the flow inside combustion chambers. It has long been known, that if the injected fuel-air mixture is given a swirl velocity component then a desirable flow pattern can be achieved. However, the underlying mechanisms, which cause this flow pattern are poorly understood, despite extensive theoretical research over the years. In the course of the project some aspects of such swirling annular jets have been studied.

In the next chapter, we will give a more extensive introduction of the project, and therefore I will only point out the main ingredients here. In Chapters 2 and 3 we will use Computational Fluid Dynamics (CFD) to get some idea of the behaviour of swirling flow, and we will also conduct a study, which aims at investigating how much an important flow property changes when the inlet geometry is varied.

In Chapter 4 we study conically self-similar solutions, which is a class of solutions to the Navier-Stokes equations. In this chapter, more traditional mathematical methods are used to prove some results for such solutions. In the penultimate chapter we compare the conically self-similar solutions to the Navier-Stokes equations with the numerically obtained simulations of combustion chamber flow in order to see to what extent an industrially relevant flow can be approximated by conically self-similar solutions. Finally, a brief summary will conclude the report.

Chapter 1

Introduction

1.1 Background

To start with let us consider a non-swirling jet emerging from an annular orifice. At some downstream position, the velocity profile of the jet will be well approximated by the profiles of Schlichting and Landau, which are treated in any introductory book on fluid mechanics.

Let us now suppose that we give our jet a gradually increasing swirl velocity. Initially, the flow pattern, shown in figure 1.1(a) will be almost unchanged compared to the non-swirling one. This remains true, until we have reached a certain degree of swirl, but then the entire flow pattern suddenly changes. The resulting flow pattern, which is illustrated in figure 1.1(b), is characterised by a large and very stable recirculation zone along the symmetry axis. This sudden change of the flow pattern is called vortex breakdown.

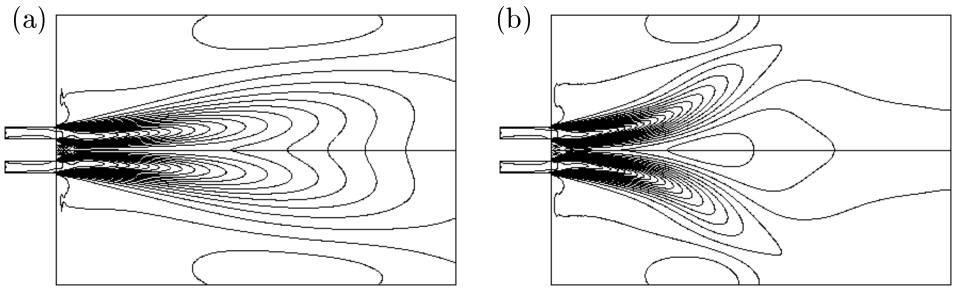

Figure 1.1: A swirling annular jet (a) before vortex breakdown and (b) after vortex breakdown. The figure shows contours of the axial velocity component of a solution obtained by CFD.

1.2 The application of swirling jets in combustion chambers

The flow pattern, which is obtained after vortex breakdown is very well suited for flow in, for example, a combustion chamber, primarily for two reasons: firstly, the large and stable central recirculation zone gives a stable flame and secondly, swirling flow has high turbulence intensity, which accelerates the vaporisation as well as the mixing. These qualities account for the frequent use of swirling jets in the design of low-emission combustion chambers, which is currently undertaken at Volvo Aero Corporation. These small gas turbines, designed for stationary, automotive and marine use are based on LPP (Lean, Pre-mixed, Pre-vapourised) - technology, i.e. air and fuel are mixed and vaporised completely prior to combustion, which yields a very clean flame with little NO_x formation.

For a given chamber geometry it is possible to make reasonably accurate predictions of the flow pattern using CFD (Computational Fluid Dynamics), but such calculations are very time consuming. However, when designing a combustion chamber, one would, of course, like to consider a wide range of different chamber geometries. Consequently, it would be desirable to obtain more general knowledge of swirling jets. For example, if there were a simple method to calculate the shape of the central recirculation zone for any geometry and any degree of swirl, the amount of numerical computation needed in the design process could be greatly reduced.

For the application of swirling jets in combustion chambers it is an absolute requirement that the flow has undergone vortex breakdown, and therefore one would like a simple criterion which determines the degree of swirl needed to achieve this. However, no such simple criterion exists. This is elucidated by the fact that quoted critical values in the literature deviate by more than a factor two. To make matters worse, as many as three different dimensionless quantities are commonly used to quantify the degree of swirl. In Chapter 3 we will discuss the possibility of obtaining a vortex breakdown criterion using any one of those three dimensionless quantities.

1.3 Vortex breakdown theory

The most commonly accepted explanation of vortex breakdown is Benjamin's conjugate state theory [1], which proposes that vortex breakdown is a transition between two different swirling flow states. Benjamin [1] also derived his Critical Equation, which determines whether or not it is possible for extremely long travelling waves to travel upstream, in order to see whether vortex breakdown has been undergone or not. Unfortunately, it is very difficult to extract useful information from Benjamin's critical equation, unless the velocity profile is uniform. This is a reasonable approximation for channel flow, but hardly for a jet. For more detailed information about Benjamin's and other vortex breakdown theories we refer to [2].

1.4 Conically self-similar solutions to the Navier-Stokes equations

In this section we will momentarily leave the discussion of combustion chambers and discuss in more general terms an alternative way of elucidating vortex breakdown, which is offered by the conically self-similar solutions to the Navier-Stokes equations. Conically self-similar solutions can be studied either in cylindrical or spherical coordinates, however, in this context, we prefer to use spherical ones, as defined in figure 1.2 . In spherical coordinates, conically self-similar solutions to the Navier-Stokes equations can be described as solutions such that the quotient of any two velocity components depends only on the azimuthal angle (θ in figure 1.2). Normally one also requires that the velocity components are $\mathcal{O}\left(R^{-1}\right)$ as $R \to \infty$, or else non-vanishing transports of linear momentum would be impossible. With this definition of conically self-similar solutions it is clear that they are axisymmetric around the x_3-axis. Henceforth, we will term the x_3-axis, the symmetry axis, and we will use the term *axial components* for any x_3-components of vectors.

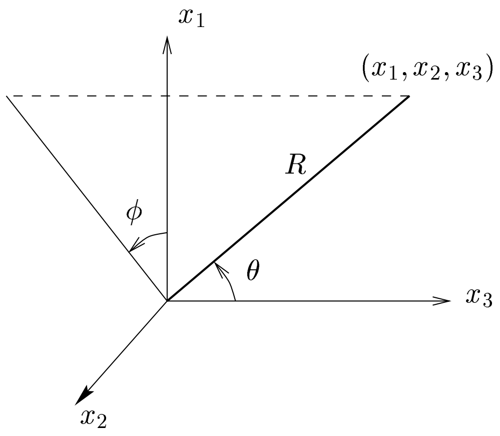

Figure 1.2: A visualisation of the standard spherical coordinates, which we use when seeking conically self-similar solutions to the Navier-Stokes equations.

In basic textbooks in fluid mechanics, see for example [3], axisymmetric non-swirling solutions to the Navier-Stokes equations are normally found by using a Stokes' streamfunction and conical self-similarity. This approach was extended to the swirling case by Long [4]. The idea is then to seek conically self-similar solutions to the Navier-Stokes equations which are characterised by a streamfunction as well as by a circulation function, i.e. to seek solutions of the form:

$$\begin{aligned} u_R &= -\frac{\nu\psi'(x)}{R}, \quad u_\theta = -\frac{\nu\psi(x)}{R\sin\theta}, \quad u_\phi = \frac{\nu\Gamma(x)}{R\sin\theta} \\ p - p_\infty &= \frac{\rho\nu^2 q(x)}{R^2}, \quad \Psi = \nu R\psi(x), \quad x = \cos\theta, \end{aligned} \tag{1.1}$$

where (R, θ, ϕ) are spherical co-ordinates (see figure 1.2), (u_R, u_θ, u_ϕ) the corresponding velocity components, p the pressure, p_∞ the atmospheric pressure and Ψ a streamfunction. We have also let a prime denote differentiation with respect to x. It may appear that (1.1) is not the most general form of a conically self-similar solution, defined as a solution which is $\mathcal{O}(R^{-1})$ and where any quotient of velocity components depend only on the azimuthal coordinate. However, if we consider only such forms of conically self-similar solutions which satisfy the continuity equation we find that (1.1) indeed is the most general form of such solutions.

In Chapter 4 we will see that for $(u_R, u_\theta, u_\phi, p)$ to be a solution to the stationary Navier-Stokes equations ψ and Γ must solve the following system of ODE's:

$$\left(1 - x^2\right)\psi' + 2x\psi - \frac{1}{2}\psi^2 = F, \tag{1.2}$$

$$\left(1 - x^2\right)F'' + 2xF' - 2F = \Gamma^2, \tag{1.3}$$

$$\left(1 - x^2\right)\Gamma'' = \psi\Gamma', \tag{1.4}$$

with suitable boundary conditions. In Chapter 4 we will prove a regularity result for conically self-similar solutions and that a conically self-similar solution is entirely determined by its behaviour on the symmetry axis. We will also use these results to show that the existence of a conically self-similar solution to the stationary Navier-Stokes equations implies the existence of a second order non-swirling correction term.

For suitable boundary conditions, it is known that there are three kinds of conically self-similar solutions:

- A near-axis jet. The fluid flows downstream in the vicinity of the symmetry axis, $x = 1$, and upstream close to the cone $x = x_c$.
- A surface jet. The fluid flows downstream along the cone $x = x_c$ and upstream along the symmetry axis.
- A two-cell flow. The fluid flows downstream along some cone $x = x_s$ and upstream both along the cone $x = x_c$ and along the symmetry axis.

Furthermore, asymptotic and numerical studies in [5] indicate that the two last solutions can exist with more swirl than the first one. Therefore, it seems that as the circulation increases above a certain value the near-axis jet breaks up, but this is precisely what happens when vortex breakdown occurs. In Chapter 5 we will discuss the relevance of conically self-similar solutions when studying swirling jets.

1.5 Numerical method

Throughout the project CFD simulations of swirling annular jets were used extensively for two main reasons. Firstly, they provided a tool to get some idea of the degree of swirl needed to reach vortex breakdown for various inlet geometries, and secondly they were used to test the relevance of the conically self-similar solutions in the study of more general swirling jets.

We used a finite volume method for axisymmetric flow with the $k-\epsilon$ turbulence model without wall-functions. The numerical method is an explicit three stage Runge-Kutta time marching method that uses an optimised local time-step. For the convective terms a third order finite volume scheme is used with upwind corrections, and a second order finite volume scheme is used for the diffusive terms. A TVD (Total Variation Diminishing) limiter is used for the k and ϵ equations. This code was developed by Lars-Erik Eriksson at the Volvo Aero Corporation, and is described in more detail in [6] and [7].

It must be emphasised that neither the comparison of various turbulence models, nor the quality of the numerical calculations have been of primary interest to us in this study. There may well be turbulence models more suited for swirling flow than the $k-\epsilon$ model without wall functions, but in all our calculations the turbulence model has been the same, and the results of the different calculations were almost exclusively compared to each other.

1.5.1 Geometry of the test cases

In all our numerical calculations we used an axisymmetric channel like the one in figure 1.3 below. In all our calculations we had $L = 1.2$ m, $\mathcal{R} = 0.13$ m and $r_o = 0.02265$ m. The values of the other parameters were varied and they will be specified later. In all our calculation, we assumed the liquid to be air at room temperature.

1.5.2 Inlet and outlet conditions

At the inlet we specified the velocity profiles, the mass flow, the total enthalpy, the turbulent intensity as well as the turbulent dissipation. We performed simulations with two different inlet velocity profiles, which we will describe in Chapter 3.

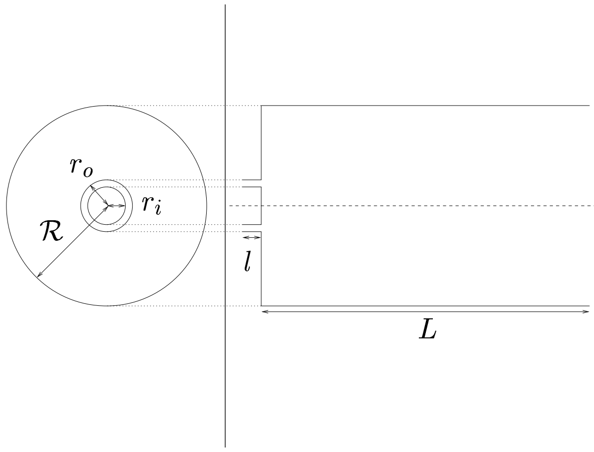

Figure 1.3: The principal geometry of a typical combustion chamber

At the outlet we only specified a constant pressure. For a swirling flow there is a radial pressure gradient, and it may be argued that a different pressure profile ought to have been used at the outlet. However, in such a long channel as ours the swirl at the outlet has decayed to a level where its effect on the pressure profile is negligible, which is the reason for our choice of a constant pressure profile at the outlet.

Chapter 2

The qualitative behaviour of swirling annular jets

In this chapter we will illustrate some features of swirling annular jets with the results from CFD simulations. In all the simulations in this chapter we used the geometry in figure 1.3 with $r_i = 0.01085$ m and $l = 0.05$ m. All the other parameters had the values given in section 1.5. In these calculations we consistently specified flat inlet velocity profiles. For this geometry we varied the degree of swirl and studied the basic changes in the flow structure, and the development of the central recirculation zone, with a special emphasis on its initial stages of development.

In the presentation we will use Re_z^j as a Reynolds number and $M^{-\frac{1}{2}}$ as a parameter indicating the degree of swirl. Both are formally defined in Chapter 3 below. Here it suffices to say that

$$M^{-\frac{1}{2}} = \frac{Re_\phi}{Re_z^j} , \tag{2.1}$$

and that Re_ϕ is a Reynolds number for the swirl velocity and Re_z^j is a Reynolds number for the axial velocity. In figure 2.1 we see the development of the axial velocity component of the flow as the degree of swirl increases. As we go from a non-swirling jet to a weakly swirling one, we notice that the jet spreads out and that the velocity gradients are smoothed. There is, however, no major difference in the actual flow structure. At vortex breakdown, we see the advent of a central recirculation zone, which grows in size as the swirl is increased further.

To study the issue of the growing central recirculation zone in more detail, we plotted the boundaries of the regions of reversed flow in figure 2.2. From this figure we see that the central recirculation zone appears as an isolated recirculation zone some distance downstream from the inlet. Even before vortex breakdown, we have both the corner recirculation zone and a tiny recirculation zone just downstream of the inlet. However, as the degree of swirl increases we see that the central recirculation zone not only grows in size, but it also travels upstream, and at some degree of swirl, the central recirculation zone merges with the tiny recirculation zone just downstream of the inlet. This phenomenon has also been observed experimentally, see for example [8].

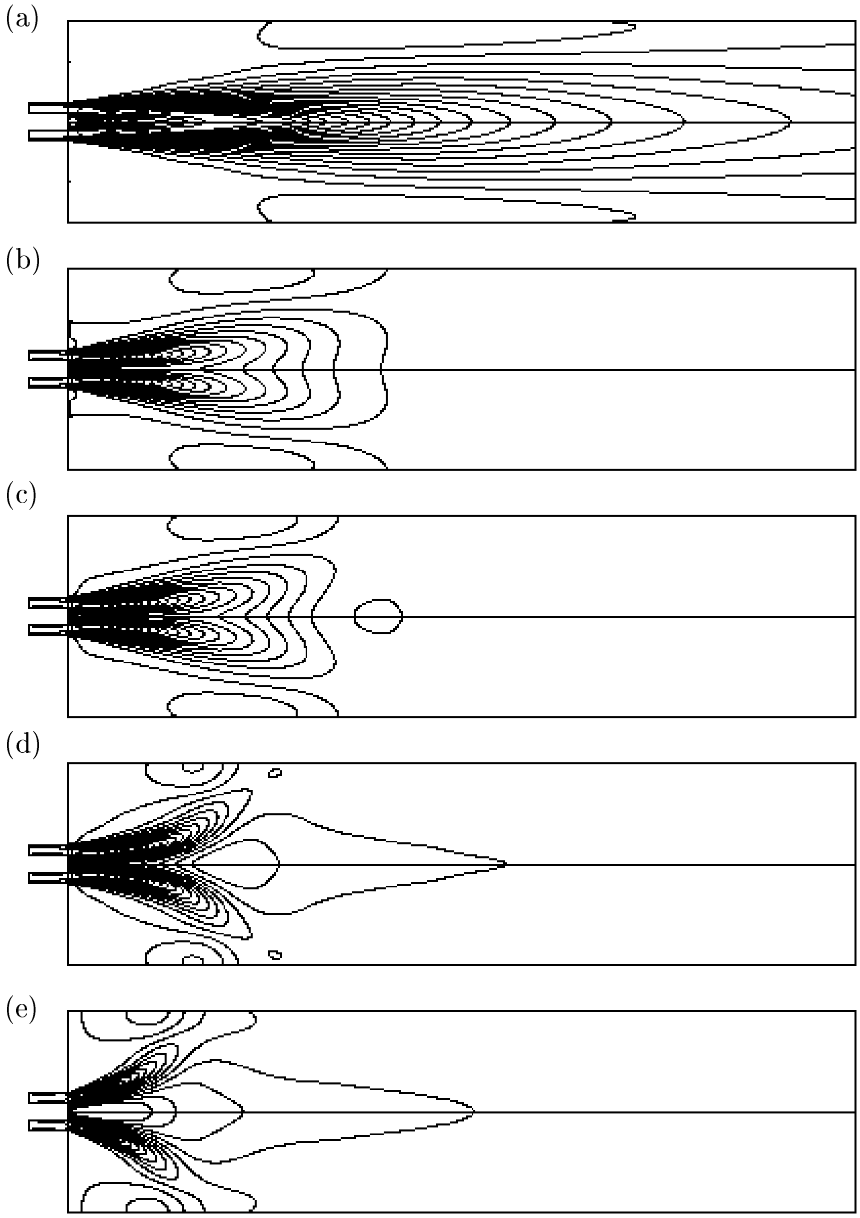

Figure 2.1: Contours of the axial velocity component at various degrees of swirl. $Re_z^j = 20300$, (a) $M^{-\frac{1}{2}} = 0$, (b) $M^{-\frac{1}{2}} = 0.401$, (c) $M^{-\frac{1}{2}} = 0.407$, (d) $M^{-\frac{1}{2}} = 0.426$ and (e) $M^{-\frac{1}{2}} = 0.561$. M and Re_z^j will be defined in Chapter 3 below.

(a)

(b)

(c)

(d)

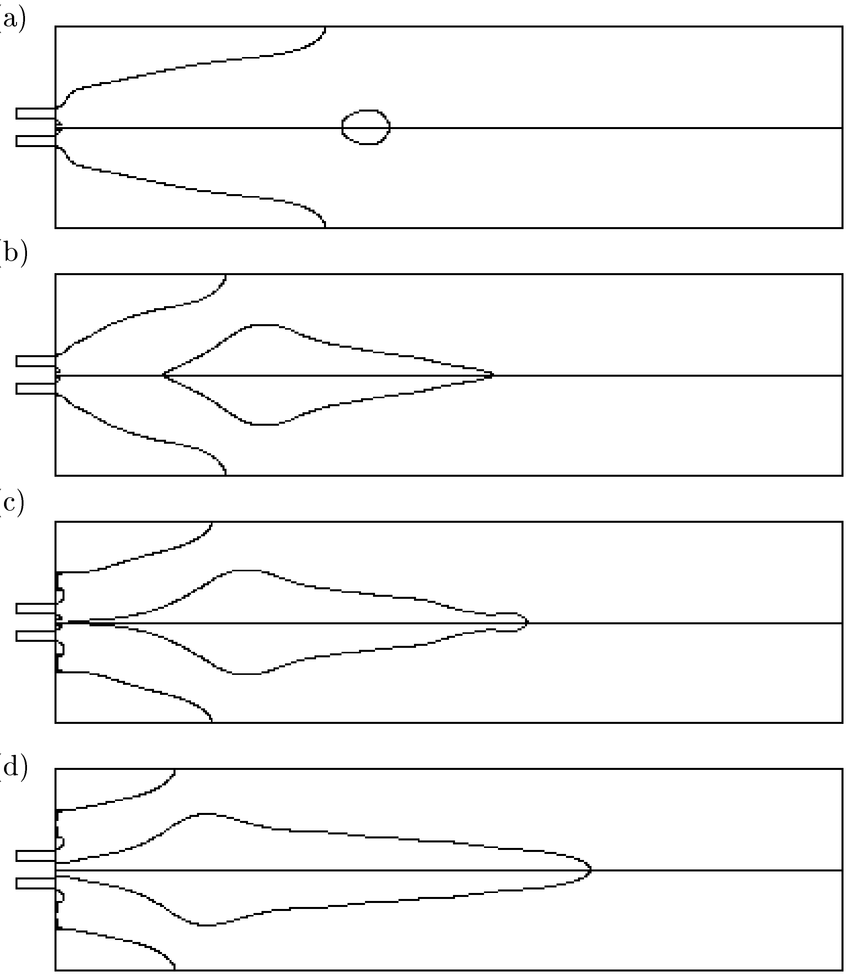

Figure 2.2: The boundaries of the domains of negative axial velocities, i.e. of the domains of reversed flow. $Re_z^j = 20300$, (a) $M^{-\frac{1}{2}} = 0.407$, (b) $M^{-\frac{1}{2}} = 0.426$, (c) $M^{-\frac{1}{2}} = 0.445$ and (d) $M^{-\frac{1}{2}} = 0.561$. M and Re_z^j will be defined in Chapter 3 below.

Chapter 3

Towards a vortex breakdown condition independent of the inflow geometry

3.1 Introduction

Already in Chapter 1 we mentioned that in the design of a combustion chamber, a swirling annular jet which does not form a central recirculation zone would be of no use. In this chapter we will study the inlet geometry dependence of various vortex breakdown conditions for swirling jets.

For non-swirling annular jets the only recirculation zone apart from the corner recirculation zone is the comparatively small recirculation zone present immediately downstream of the inlet. In Chapter 1 we defined vortex breakdown as the abrupt advent of an additional recirculation zone on the symmetry axis. This causes the flow structure to change from that in figure 1.1(a) to that in figure 1.1(b). Vortex breakdown has frequently been studied experimentally, see for example [9] or [8]. At this point we should stress that by vortex-breakdown we will not refer to a sudden change of the flow properties around some point in physical space, but rather to an abrupt change of the entire flow pattern around some value in parameter space. Henceforth, we will call the degree of swirl at which vortex breakdown occurs, the critical degree of swirl. Remember that in Chapter 2 we saw numerically that if the swirl is only marginally above the critical degree of swirl, we have at least two separated regions of reversed flow on the symmetry axis, but as we continue to increase the swirl the downstream zone will move upstream until the two zones merge. This numerical behaviour is consistent with empirical observations, see for example [8].

As mentioned in Chapter 1, quantitative comparison between the different studies of swirling jets is difficult since no less than three different dimensionless numbers are commonly used to characterise the degree of swirl.

Notwithstanding the practical difficulties this lack of standardisation brings, the main problem is that at least two of these dimensionless numbers do not include all the information needed to predict when vortex breakdown occurs. To illustrate how crucial the choice of the correct dimensionless number is, consider an ordinary non-swirling jet emerging from a circular orifice of radius R, with an almost constant velocity profile. At some distance from the orifice the jet is described by the well-known self-similar profiles found by Schlichting [10] (for the boundary-layer equations) and by Landau [11] (for the full Navier-Stokes equations). A common feature of both these solutions is that the angle of expansion of the jet far away from the orifice is entirely determined by the axial momentum of the jet and the viscosity of the fluid. If we tried to calculate this angle from say the mass flow we would obtain a complicated expression involving the radius of the orifice a, as well as the velocity profile at the inlet. In fact, by reducing a towards zero and increasing the velocity u of the jet as $\frac{1}{\sqrt{a}}$, we can obtain an arbitrarily small mass flow without changing the properties of the jet far from the orifice.

The basic geometry of a combustion chamber typically looks like the flow domain depicted in figure 1.3. It can be argued that if $\mathcal{R}/r_o \approx 1$, jet theory will not be appropriate since we essentially have a swirling channel flow. Such flows undergo vortex breakdown at some degree of swirl as is shown experimentally in [12] and [13], and for such flows Benjamin's [1] vortex breakdown theory applies. On the other hand, if $\mathcal{R}/r_o >> 1$ the flow should behave essentially like a jet. Moreover, while it is true that jet theory only treats unconfined flow, experimental measurements by Sheen *et al.* [8] show that the degree of swirl required to induce the vortex breakdown is the same for an unconfined case as for a confined case with $\mathcal{R}/r_o \approx 3$. This suggests that, at least for moderately confined cases, vortex breakdown is essentially a jet phenomenon. Hence, we will in this paper use jet theory to discuss the appropriateness of the different dimensionless swirl numbers from a theoretical point of view. To try to single out one of the parameters, we will, in addition, use numerics to see how much the critical degree of swirl, as expressed in the different dimensionless numbers, changes when we alter the inlet geometry or the inlet velocity profiles.

3.2 The different dimensionless numbers used to characterise swirl

The dimensionless numbers used to characterise the degree of swirl are of three main types. Firstly, it can be a quotient between the flux of angular momentum and the flux of axial momentum multiplied by a typical length scale, secondly it can be a quotient between the circulation and a typical velocity multiplied by a typical length scale and finally it can be a quotient between the flux of axial momentum and the circulation squared, *i.e.*

expressed mathematically the three main types are:

$$S = \frac{\int_0^{r_o} UWr^2dr}{r_o\int_0^{r_o} U^2rdr} \;, \tag{3.1}$$

$$\beta = \frac{K_c}{u_0 r_i} \text{ and} \tag{3.2}$$

$$M = \frac{J_z}{\rho K_c^2} \;, \tag{3.3}$$

where r_o is the outer and r_i the inner radius of the orifice, U the axial and W the azimuthal velocity, K_c a characteristic circulation of the incoming fluid, and ρ the density. Finally, u_0 and J_z are given by:

$$u_0 = \frac{Q}{\rho A} = \frac{2\int_{r_i}^{r_o} Urdr}{r_o^2 - r_i^2} \text{ and} \tag{3.4}$$

$$J_z = 2\pi\rho\int_0^\infty \left\{U^2 + \frac{(p-p_\infty)}{\rho} - 2\nu\frac{\partial U}{\partial z}\right\} rdr \;. \tag{3.5}$$

Here, Q is the mass flow, A the surface area of the orifice, p the pressure, p_∞ the atmospheric pressure and ν the viscosity. Note that for intensive flow the the denominator in S is approximately equal to J_z. The parameter S is most often found in experimental [8] and numerical [14] papers. β is used in Benjamin's vortex breakdown theory and consequently in various theoretical and experimental articles and M is primarily used in articles which use conically self-similar solutions to describe swirling jets in unbounded space.

To summarize, all three of the dimensionless numbers in (3.1)-(3.3) measure the ratio between either J_z or Q and either L_z and K_c. The quantities L_z and Q are conserved in a control volume, J_z decays at walls but is conserved in control volumes away from the walls and K_c is conserved on streamsurfaces.

It seems reasonable that a swirl number should be the ratio of the Reynolds numbers in the axial and azimuthal directions. This point of view shows that β is the natural parameter if one treats the flow as essentially a channel flow, and that M is the natural parameter if the flow is essentially a jet flow. Indeed, if we use $Re_\phi = \frac{K_c}{\nu}$ as the Reynolds number for the azimuthal flow, which we can do since the circulation on a streamsurface is conserved and has the dimension of viscosity, and if we take the axial Reynolds number of a non-swirling jet in unconfined space, $Re_z^j = \frac{J_z^{1/2}}{\rho^{1/2}\nu}$,we find that $M = \left(\frac{Re_z^j}{Re_\phi}\right)^2$. Alternatively, if we take the Reynolds number of the flow in an annular channel, $Re_z^c = \frac{Qr_o}{\rho A\nu}$ we find that $\beta = \frac{Re_\phi r_o}{Re_z^c r_i}$. The factor r_o/r_i in β takes into account which proportion of the flow initially swirls. If we similarly view S as a quotient of an azimuthal and axial Reynolds number, we obtain the azimuthal Reynolds number $Re_\phi^* = \frac{L_z^{1/2}}{(\rho r_o)^{1/2}\nu}$, which has the undesirable property that one of the quantities defining it, the characteristic radius of swirl r_o, changes in the process of vortex breakdown.

The quantities involved in the dimensionless number S, J_z and L_z, are precisely those conserved in the solution for swirling jets developed by Loitsyanskii [15] and others. It is, however, known that a Loitsyanskii jet cannot produce a zone of axially reversed flow [16]. Consequently, the theoretical support for the use of S to describe vortex breakdown is rather weak. By contrast, both of the dimensionless numbers β and M do have theoretical support. The former from vortex breakdown theory, and the latter from the conically self-similar solutions (mentioned in Chapter 1, and described in more detail in Chapter 4), and both of these methods offer possible predictions for vortex breakdown.

For a given geometry and inlet profile S, β and M are equivalent, and as we change the axial Reynolds number, the critical values of the different parameters will trace curves which only differ by a constant factor, and such curves have been found experimentally for instance in [8] and [13], and they reveal that once the axial Reynolds number is moderately large then the critical value of swirl is rather insensitive to changes in the axial Reynolds number. However, if we change the geometry or the inlet profile these critical values change, and the less relevant the dimensionless number for vortex breakdown, the more sensitive should the parameter be to such changes. In this chapter we will use numerics to study is issue.

3.3 Geometry of the test cases

As already stated in Chapter 1 we used an axisymmetric channel like the one in Figure 1.3 in all our calculations. We simulated swirling jets for two different inlet geometries, and for one geometry we used two different inlet profiles, which gives us three cases in all. Recall that we consistently used $L = 1.2$ m, $\mathcal{R} = 0.13$ m and $r_o = 0.02265$ m. The values of the other parameters are given for the different cases in table 3.1. The parameter l can appear to have little influence on the flow inside the combustion chamber, however, when obtaining solutions using CFD, a proper choice of the length of the inlet section appeared to be of some importance.

When we used the flat profile we set both the axial and azimuthal velocities to be constant over the entire inlet. In the case of the laminar profile we set both the axial and azimuthal velocity profiles to the laminar profile of the axial flow in an annular channel when there is no swirl. This profile is given by

$$u(r) = C\frac{r_o^2 \ln\frac{r}{r_i} + r^2 \ln\frac{r_i}{r_o} + r_i^2 \ln\frac{r_o}{r}}{ln\frac{r_o}{r_i}} \; . \tag{3.6}$$

From the profiles given in [8] it appears that this profile approximates the axial velocity profile well even in the case of moderate swirl. For the azimuthal velocity profile this approximation is somewhat less accurate, but the profiles in [8] show that this profile changes significantly with the amount of swirl present, which makes the determination of a realistic profile difficult.

	Geometry r_i (m)	l (m)	Velocity Profile
Case 1	0.01085	0.05	flat
Case 2	0.01085	0.05	laminar
Case 3	0.01965	0.01	flat

Table 3.1: Definition of the geometry and the inlet profile of the various cases for which numerical simulations were performed.

3.4 Results and discussion

To compare S, β and M fairly, they should all depend on the axial Reynolds number in the same way. For that reason we do not compare them directly, but form quantities similar to each of them, but on the form Re_ϕ/Re_z. Such quantities are:

$$S^{\frac{1}{2}} = \frac{Re_\phi^*}{Re_z^j} \tag{3.7}$$

$$\beta = \frac{Re_\phi}{Re_z^c}\frac{r_o}{r_i} \tag{3.8}$$

$$M^{-\frac{1}{2}} = \frac{Re_\phi}{Re_z^j} \tag{3.9}$$

and these are the quantities we will compare to each other.

3.4.1 The critical degree of swirl

In all our cases we started with an almost swirl-free jet, and gradually increased the swirl. For swirl lower than the critical degree the flow pattern typically looked like that in figure 1.1(a), whereas it typically looked like that in figure 1.1(b) once the critical degree of swirl had been exceeded.

We measured all quantities in the chamber at a section 0.005 downstream of the orifice. The characteristic circulation posed a difficulty in that it is not clear what circulation to take as the characteristic, but we selected the maximum circulation at the section 0.005 downstream of the orifice.

	Critical Degree of Swirl			Re numbers	
	$S^{\frac{1}{2}}$	β	$M^{-\frac{1}{2}}$	Re_z^j	Re_z^c
Case 1	$0.695 - 0.700$	$1.266 - 1.286$	$0.401 - 0.407$	20 300	13 500
Case 2	$0.701 - 0.717$	$1.180 - 1.251$	$0.372 - 0.391$	18 500	12 100
Case 3	$0.544 - 0.562$	$0.327 - 0.353$	$0.330 - 0.355$	23 400	27 300

Table 3.2: The critical degree of swirl for the different cases as expressed in the different parameters.

From table 3.2 it is evident that the geometry dependence of the critical degree of swirl is considerably less for M than for β, and appreciably less than for S. It is known from [8], [13] that the Reynolds number dependence of the critical degree of swirl is weak for Reynolds numbers above 5000. Therefore the high channel Reynolds number for Case 3 can hardly account for the difference in the critical degree of swirl when expressed in β. We also see that the inlet profile dependence of the critical degree of swirl is too weak to support any reasonable conclusion. It must be noted, however, that whereas the inlet profile in Case 1 and Case 2 only varies moderately, the inlet geometry in Case 3 differs considerably from that in Case 1 and Case 2.

Chapter 4

Some mathematical aspects of conically self-similar solutions to the Navier-Stokes equations

4.1 Introduction

We have already seen in Chapter 1 that conically self-similar solutions to the Navier-Stokes equations are solutions on the form (1.1). The first such conically self-similar solution to the Navier-Stokes equations was the asymptotic solution for a non-swirling jet in the whole space derived by Landau [11]. This solution generalised Schlichting's [10] for the boundary layer equations, and is given on the form (1.1) by

$$\psi(x) = 2\frac{1-x^2}{A-x}, \quad \Gamma(x) = 0, \quad q(x) = -4\frac{1-Ax}{(A-x)^2}, \tag{4.1}$$

where A is a constant, which can be used to specify the total flux of axial momentum through a sphere of arbitrary radius.

A drawback that this non-swirling self-similar jet solution shares with Schliching's solution is that neither of them admits any mass flow. For the Landau solution (4.1) this can be amended by adding higher order terms, as outlined in [17]. This paper also discusses the construction of a full solution to the general problem of non-swirling jets.

The first attempt to construct a solution for swirling jets was made by Loitsyanskii [15], who used the boundary-layer equations and the conservation of angular momentum to study swirling jets. An equivalent solution was constructed by Görtler [18], who considered only weak swirl, which allowed him to neglect the centrifugal force term. Tsukker [19] used the full Navier-Stokes equations and the conservation of angular momentum to modify the

Landau solution for the swirling case. All of these solutions have the property that the swirling (azimuthal) velocity decays faster than the axial and radial velocities, and none of them allow a central recirculation zone.

The use of conservation of circulation on streamsurfaces, in the derivation of velocity profiles for swirling jets, traces back to Long [4] and [20], and independently to Goldshtik [21]. In these articles swirling conically self-similar solutions appeared for the first time. With different boundary conditions this class contains a variety of vortex solutions, such as that of Serrin's [22], and a modification of Landau's solution, which includes swirl and conserves the circulation on streamsurfaces [16]. A summary of these solutions can be found in [23], and a number of mathematical and physical properties of these solutions were studied in [24] and in [25]. In these articles it was found that both one- and two-cell flow patterns could occur, which shows that the class of conically self-similar solutions contains solutions resembling those in a swirling jet both before and after vortex breakdown. A study of conical vortices in the context of conservation laws was conducted by Paull and Pillow [26]. Lately, Shtern and Hussain have used both numerics and asymptotic analysis to study conically self-similar jets in a half-space [27] as well as in cones bounded by streamsurfaces [5].

In this chapter we will prove two main results. Firstly, we will prove that any conically self-similar solution is real analytic and also that it is entirely determined by its behaviour on the symmetry axis. This result provides some mathematical justification for a common method for calculating conically self-similar solutions numerically. Secondly, we will use this result to prove that for any conically self-similar solution there exists a second order non-swirling correction term. For Long's problem [4] and [20], which is a conically self-similar solution to the boundary-layer equations with a set of boundary conditions similar to, but different from, the ones we will use, such a correction term was found numerically by Burggraf and Foster [28]. For physical reasons they also claimed that their correction term did not give any second order contribution to the total flux of axial momentum. In this chapter we will prove that this claim is correct for the generalisation to the Navier-Stokes equations of Long's problem made by Shtern and Hussain [5]. However, we will also see that for a conically self-similar solution in a cone bounded by a streamsurface, there is, in general, a second order contribution to the total flux of axial momentum.

In a recent article Drazin, Banks and Zaturska [29] studied the general problem of finding correction terms to Long's problem generalised to the full Navier-Stokes equations. They used cylindrical coordinates and stability theory and they found explicit expressions for non-swirling correction terms of m:th order ($m \geq 2$) in the Stokes limit (the low Reynolds number limit). However, even though they stated the vanishing of the second order contribution to the total flux of axial momentum, as a requirement for any second order correction term to their conically self-similar solution, they never actually proved that this is the case for the correction terms they found. Our results are more general in that they are applicable for any Reynolds number, and they also extend to any flow domain which is bounded by a conical streamsurface. It should be noted, however, that whereas Drazin-Banks and Zaturska used Long's boundary conditions, which are applicable when cylindrical coordinates are used in a half-space, we will, when discussing Long's problem, use the similar, albeit different, boundary conditions of Shtern and Hussain's [5] extension of Long's problem to the full Navier-Stokes equations and the entire space. These boundary conditions, which we will present below, are more suitable when using spherical coordinates.

4.2 The basic model

In Section 1.4 we defined conically self-similar solutions to the Navier-Stokes equations, and we also discussed the physical meaning of the Ansatz (1.1). Since one of our main aims in this chapter is to prove that any conically self-similar solution has a second order non-swirling correction term, we will modify the Ansatz (1.1) to include such a term. Consequently, we will in the established manner look for axisymmetric solutions to the stationary incompressible Navier-Stokes equations (see Appendix A) on the form:

$$\begin{aligned} u_R &= -\frac{\nu\psi'(x)}{R} - \frac{\nu z'(x)}{R^2}, \quad u_\theta = -\frac{\nu\psi(x)}{R\sin\theta}, \quad u_\phi = \frac{\nu\Gamma(x)}{R\sin\theta}, \\ p - p_\infty &= \frac{\rho\nu^2 q(x)}{R^2} + \frac{\rho\nu^2 g(x)}{R^3}, \quad \Psi = \nu R\psi(x) + \nu z(x), \end{aligned} \tag{4.2}$$

where $x = \cos\theta$ and a prime denotes differentiation with respect to x.

We will now begin by finding out which conditions ψ, Γ and q must satisfy for (1.1) to be a conically self-similar solution to the Navier-Stokes equations. The derivation below is standard in the field, and the results we obtained are consistent with those of other workers. In the literature, a rather detailed derivation can be found in [22]. While we are deriving the conditions for ψ, Γ and q to be a conically self-similar solution to the Navier-Stokes equations we will derive conditions for z and g to be second-order non-swirling correction terms. In part this derivation is presented in the literature. For the case of a non-swirling conically self-similar solution in entire space this derivation was performed in [17], and for the boundary-layer equations and cylindrical coordinates a similar derivation appears in [28].

As mentioned in Chapter 1 all solutions on the form (4.2) automatically satisfy the continuity equation. When we substitute (4.2) into the radial equation (A.2) and identify first the terms of order R^{-3}, and then those of order R^{-4}, we obtain

$$\left(1 - x^2\right)\psi''' - 2x\psi'' - \frac{1}{2}\left(\psi^2\right)'' - \frac{\psi^2 + \Gamma^2}{1 - x^2} - 2q = 0 \text{ and} \tag{4.3}$$

$$\left(1-x^2\right)z''' - 2xz'' - \psi z'' - 3\psi' z' - 3g \;=\; 0 \qquad (4.4)$$

respectively. If we now substitute our Ansatz into azimuthal equation (A.3) we obtain

$$\left(1-x^2\right)\psi'' + \psi\psi' + \frac{x}{1-x^2}\left[\psi^2+\Gamma^2\right] + q'\left(1-x^2\right) \;=\; 0 \text{ and} \qquad (4.5)$$

$$g' + 2z'' \;=\; 0\,. \qquad (4.6)$$

Finally, substitution into the equation for u_ϕ (A.4) shows that this equation is satisfied if and only if

$$\left(1-x^2\right)\Gamma'' = \psi\Gamma'\,. \qquad (4.7)$$

If we differentiate (4.3) and use the expression for q' given from (4.5) we obtain the fourth order equation

$$\left(1-x^2\right)^2\psi^{IV} - 4x\left(1-x^2\right)\psi''' - \frac{1}{2}\left(1-x^2\right)\left(\psi^2\right)''' = \left(\Gamma^2\right)'\,. \qquad (4.8)$$

We can write (4.8) in the form

$$\left(1-x^2\right)\left\{\left(1-x^2\right)\psi' + 2x\psi - \frac{1}{2}\psi^2\right\}''' = \left(\Gamma^2\right)'\,, \qquad (4.9)$$

and then follow Goldshtik [21] and introduce the auxiliary function F defined by

$$F = \left(1-x^2\right)\psi' + 2x\psi - \frac{1}{2}\psi^2\,, \qquad (4.10)$$

which turns (4.9) into

$$\left(1-x^2\right)F''' = \left(\Gamma^2\right)'\,. \qquad (4.11)$$

This equation was integrated in Sozou [30] to yield

$$\left(1-x^2\right)F'' + 2xF' - 2F = \Gamma^2 + C\,. \qquad (4.12)$$

In the next subsection we shall see that a necessary condition for u_θ and for u_ϕ to remain finite on the symmetry axis ($x=1$) is that $C=0$. However, there are interesting cases where the boundary conditions are such that the velocity components are singular on the symmetry axis, for example Serrin's problem [22], where we do not have that $C=0$, and in these cases one might prefer to use (4.11) rather than (4.12). However, we will not treat these cases, and henceforth we will assume that $C=0$, which implies that we have the following system of ODEs for the highest order terms in (4.2):

$$\left(1-x^2\right)\psi' + 2x\psi - \frac{1}{2}\psi^2 \;=\; F\,, \qquad (4.13)$$

$$\left(1-x^2\right)F'' + 2xF' - 2F \;=\; \Gamma^2\,, \qquad (4.14)$$

$$\left(1-x^2\right)\Gamma'' \;=\; \psi\Gamma'\,. \qquad (4.15)$$

To find the equation for the second order non-swirling correction z first notice that (4.6) implies that

$$g + 2z^{'} = c \ . \tag{4.16}$$

Substitution of this into (4.4) now yields

$$\left(1 - x^2\right) z^{'''} - 2xz^{''} - \psi z^{''} - 3\psi^{'} z^{'} + 6z^{'} = 3c \ . \tag{4.17}$$

Notice that this is an equation in $z^{'}$, and thus it only determines z modulo an additive constant.

4.2.1 Boundary conditions

There are several possible choices of boundary conditions, but the ones we will consider are the ones most commonly used in the literature. These boundary conditions are obtained if we assume that we do not have any flow sources on the axis, except at the origin, which implies that

$$\Gamma(1) = \psi(1) = 0 \ . \tag{4.18}$$

For the radial velocity to be bounded outside a neighbourhood of the origin we require that $\left|\psi^{'}(1)\right| < \infty$. If we substitute these conditions into (4.13) and its derivative, we obtain boundary conditions for F,

$$F(1) = F^{'}(1) = 0 \ . \tag{4.19}$$

When the conditions (4.18)-(4.19) are substituted into (4.12) we find that $C = 0$.

We furthermore assume that the swirling flow is driven by a constant circulation along some fixed conical streamsurface $x = x_c$ (throughout the report the subscript c has no connection to any other c's.) which implies that

$$\begin{aligned} \psi(x_c) &= 0 \text{ and} & (4.20) \\ \Gamma(x_c) &= \Gamma_c \ . & (4.21) \end{aligned}$$

Since the system of equations (4.13)-(4.15) is symmetric with respect to the sign of Γ, the sign is immaterial, and we will henceforth assume that $\Gamma_c \geq 0$.

From (4.2) we find that to avoid flow sources on the axis we need not impose any other condition on $z^{'}$ than $\left|z^{'}(1)\right| < \infty$.

The last condition to be specified is the total axial flow force J_z, and this will the subject of the next subsection.

4.2.2 The total axial flow force

The total axial flow force acting at a spherical section $0 \le \theta \le \theta_c$ and $r =$const is given by

$$
\begin{aligned}
J_z &= 2\pi\rho r^2 \int_{x_c}^{1} j dx \ , & (4.22)\\
\rho j &= \Pi_{rr} x - \Pi_{r\theta}\sqrt{1-x^2} \ , & (4.23)\\
\Pi_{rr} &= \rho u_r^2 + p - 2\rho\nu \frac{\partial u_r}{\partial r} \ , & (4.24)\\
\Pi_{r\theta} &= \rho u_r u_\theta - \rho\nu \left[\frac{1}{r}\frac{\partial u_r}{\partial \theta} + r\frac{\partial}{\partial r}\left(\frac{u_\theta}{r}\right)\right] \ . & (4.25)
\end{aligned}
$$

If we substitute (4.2) into these formulae we obtain

$$
\begin{aligned}
J_z &= 2\pi\rho\nu^2 \left(J_1 + \frac{J_2}{r}\right) + \mathcal{O}\left(r^{-2}\right) \ , \text{ where} & (4.26)\\
J_1 &= \int_{x_c}^{1} \left\{ \left(1-x^2\right)\psi'' + x\left[\psi'\left(\psi'-2\right)+q\right] + \psi\left(2-\psi'\right)\right\} dx, & (4.27)\\
J_2 &= \int_{x_c}^{1} \left\{ \left(1-x^2\right) z'' + z'\left(2x\psi' - 6x - \psi\right) + cx \right\} dx \ , & (4.28)
\end{aligned}
$$

and where c is as in (4.16). We can calculate q from (4.3) or from the simplified expression

$$
q = \frac{2x\psi - xF' - \psi^2}{1-x^2} \ . \qquad (4.29)
$$

We would like to use J_z as a fundamental flow parameter. A complication arises if we choose $x_c = -1$, in which case the integral in (4.27) diverges, as was originally found by Goldshtik [16]. He also proposed that when $x_c = -1$ we use, instead of J_z, J_0 where the integration is only over the hemisphere with non-negative z-values, i.e.

$$
\begin{aligned}
J_0 &= 2\pi\rho\nu^2 \int_0^1 j dx \ , & (4.30)\\
&= 2\pi\rho\nu^2 \left(J_{1,0} + \frac{J_{2,0}}{r}\right) + \mathcal{O}\left(r^{-2}\right) \ , & (4.31)
\end{aligned}
$$

where j is as in (4.23) and $J_{1,0}$ and $J_{2,0}$ are defined in the same way as J_1 and J_2. Shtern and Hussain [5] showed that this is a generalisation of Long's problem [20] for the full Navier-Stokes equations in the whole space. As already mentioned in Section 4.1 we should emphasise that the boundary condition in Shtern and Hussain's generalisation of Long's problem are not exactly the same as those in Long's original problem. However, Shtern and Hussain [5] showed that their generalisation of Long's problem shared most relevant properties with Long's original problem.

When we include the non-swirling second order term $z^{'}$, there is a new problem. We need to control J_2. Indeed, for the problem mentioned in the previous paragraph $J_{2,0}$ must be zero, or else the second order non-swirling correction term would be of little physical interest. Burggraf and Foster [28] claimed that this was the case for their second-order non-swirling correction term to the conically self-similar solutions of the boundary layer equations, but they provided no mathematical argument to support their claim. In this chapter we will provide such an argument.

First of all we will prove the following theorem, which gives us a way to calculate J_2.

Theorem 1 *Let* $z^{'} \in C^2\left((x_c,1)\right)$ *be a solution to (4.17) and let* $\psi \in C^1\left((x_c,1)\right)$ *be part of a solution to (4.13)-(4.15).*
(a) If $x_c \neq -1$ *then*

$$\begin{aligned} J_2 &= \lim_{x \to 1^-} x\left[\left(1-x^2\right)z^{''} - \psi z^{'}\right] - \\ &- \lim_{x \to x_c^+} x\left[\left(1-x^2\right)z^{''} - \psi z^{'}\right] - \left(1-x_c^2\right)c \,. \end{aligned} \tag{4.32}$$

(b) If $x_c = -1$ *then*

$$J_{2,0} = \lim_{x \to 1^-} x\left[\left(1-x^2\right)z^{''} - \psi z^{'}\right] - c \,. \tag{4.33}$$

Remark 1: Notice that in case (b) we want to prove that $J_{2,0} = 0$. If we can prove that $z^{'} \in C^1\left((x_c,1]\right)$, Theorem 1 tells us that $J_{2,0} = 0$ if and only if $c = 0$. Consequently, the proof of Burggraf and Foster's claim is reduced to proving sufficient regularity of the solution to (4.17).
Remark 2: If $c = 0$, $x_c \neq -1,\ 0,\ 1$ and $z^{'} \in C^1\left((x_c,1]\right)$ then $J_2 = 0$ if and only if $z^{''}(x_c) = 0$. Numerical solutions suggest that this is not the case. Therefore it appears that in general $J_2 \neq 0$.

Proof. To begin with let us note that

$$\frac{d}{dx}\left\{x\left(1-x^2\right)z^{''}\right\} = x\left(1-x^2\right)z^{'''} - 2x^2 z^{''} + \left(1-x^2\right)z^{''} \,. \tag{4.34}$$

If we now multiply (4.17) by x and use (4.34) we obtain

$$\begin{aligned} &\frac{d}{dx}\left\{x\left[\left(1-x^2\right)z^{''} - \psi z^{'}\right]\right\} = \\ &= \left(1-x^2\right)z^{''} + z^{'}\left(2x\psi^{'} - 6x - \psi\right) + 3xc \,. \end{aligned} \tag{4.35}$$

If we integrate this expression from x_c to 1 we obtain (a). To obtain (b) we integrate (4.35) from 0 to 1, which gives

$$\begin{aligned} J_{2,0} &= \left[x\left(1-x^2\right)z^{''} - x\psi z^{'} - x^2 c\right]_0^1 &(4.36)\\ &= \lim_{x \to 1^-} x\left[\left(1-x^2\right)z^{''} - \psi z^{'}\right] - c \,, &(4.37) \end{aligned}$$

where the last equality holds since z'' and ψ are continuous in $(-1,1)$ and consequently they are bounded at $x=0$. $\square$

4.3 On the existence of solutions to the conically self-similar equations

To prove the existence of conically self-similar solutions with no flow sources on the symmetry axis, we must answer the question of the existence of a bounded solution to (4.13)-(4.15) with boundary conditions (4.18)-(4.21) for a given Γ_c, and we must require that this solution has the prescribed value of J_z. This is, in fact, an intricate question. For similar problems it was first considered by Long [4] and Goldshtik [21]. The most clarifying result is due to Yih *et al* [24], who adapted a technique of Serrin's [22] to this problem. They did not, however, use J_z as a fundamental flow parameter, but instead a parameter T, which is the degree of freedom left when (4.11) is integrated and the boundary conditions (4.19) are imposed, i.e.

$$F = -\left(1-x\right)^2 \int_{x_c}^{x} \frac{t\Gamma^2 dt}{\left(1-t^2\right)^2} - x\int_{x}^{1} \frac{\Gamma^2 dt}{\left(1+t\right)^2} - \frac{T\Gamma_c^2}{2}\left(1-x\right)^2 \ . \tag{4.38}$$

With T defined in this way Yih *et al* [24] proved the following result

Theorem 2 *(Yih, Wu, Garg and Leibovich)*
For any Γ_c and any $x_c \in [0,1)$ there exist T_1, T_2, $T_1 > T_2$ such that for all $T \geq T_1$ there exist bounded solutions to (4.13)-(4.15) which satisfy the boundary conditions (4.18)-(4.21). Furthermore, for all $T < T_2$ such solutions do not exist.

It should be noted that Yih *et al* treated any $x_c \in (-1,1)$ and although they proved several interesting results for this case, including a generalisation of the non-existence result above, they did not provide a proper proof of the existence of a solution for negative x_c. In addition, they also gave the following estimates of T_1 and T_2:

$$T_1 \leq -\frac{\pi^2\left(1+x_c\right)^2}{\Gamma_c^2\left(1-x_c\right)^2} \tag{4.39}$$

$$T_2 \geq \min_{x_1}\left\{\frac{\pi^2\left(1+x_1\right)^2}{\Gamma_c^2\left(x_1-x_c\right)^2} + \frac{x_1 H^\dagger\left(x_1\right)}{1-x_1} - \frac{x_c^2 H^\dagger\left(x_c\right)}{1-x_c^2}\right\} , \tag{4.40}$$

where

$$H^\dagger\left(x\right) = \begin{cases} 1, & \text{for } x>0 \\ 0, & \text{for } x\leq 0 \end{cases} \ . \tag{4.41}$$

When this theorem is applicable our original problem is reduced to the study of the map

$$\mathcal{J} : \mathbb{R}^2 \times (-1,1) \to \mathbb{R} \ , \text{ defined by} \tag{4.42}$$

$$\mathcal{J}\left(T,\Gamma_c,x_c\right) = J_z \ . \tag{4.43}$$

An extensive asymptotic and numerical study by Shtern and Hussain [5] suggests that in general this map is neither injective nor surjective. Indeed, their asymptotic study shows that for each Γ_c and x_c there is a minimum value of J_z, and for some values of J_z, Γ_c and x_c as many as five different solutions exist.

4.4 Regularity and uniqueness of conically self-similar solutions

In this section we will assume the existence of conically self-similar solutions, and we will prove, the apparently new result, that any such solution must be both real analytic in $(x_c, 1)$ and analytic in some disc around $x = 1$ in the complex plane. In the next section we will use this result to prove the existence of a solution to (4.17).

Furthermore, in this section we will also prove that a conically self-similar solution is uniquely determined by the values of $\psi'(1)$, $F''(1)$ and $\Gamma'(1)$. This is a non-trivial statement since the system (4.13)-(4.15) has a singularity at $x = 1$, and neither standard Lipschitz arguments nor power series expansions can be used directly to establish uniqueness in C^1. A common way to find conically self-similar solutions numerically, is to use use tentative values of $\psi'(1)$, $F''(1)$ and $\Gamma'(1)$ and then to use a shooting method to fulfill the boundary conditions at $x = x_c$, see for example [27] and [5]. It is evident that this method requires that a conically self-similar solutions are uniquely determined by the values of $\psi'(1)$, $F''(1)$ and $\Gamma'(1)$, and therefore, the result we are about to state provides some mathematical justification of this numerical method.

Theorem 3 *(Uniqueness and Regularity)*
For any solution to (4.13)-(4.15) such that $\psi \in C^1((x_c, 1))$, $F \in C^2((x_c, 1))$ and $\Gamma \in C^2((x_c, 1))$, and which satisfies the boundary conditions (4.18)-(4.21) including the condition $\left|\psi'(1)\right| < \infty$, there exists a domain $\Omega \subset \mathbb{C}$ which contains $(x_c, 1)$ as well as a ball $B(1, r)$ for some $r > 0$, such that ψ, F and Γ in fact belong to $A(\Omega)$. Furthermore, this solution is uniquely determined by its values $\psi'(1)$, $F''(1)$ and $\Gamma'(1)$. Here $A(\Phi)$ denotes the class of analytic (holomorphic) functions in Φ, and $B(a, r)$ is the disc in the complex plane with centre at a and radius r.

The proof of this theorem will preoccupy us for the remainder of this section, and it will consist of a sequence of lemmata and propositions. First we will prove the real analyticity of a conically self-similar solution outside the singularity at $x = 1$.

Lemma 1 *Any solution to (4.13)-(4.15) such that* $\psi \in C^1((x_c, 1))$*,* $F \in C^2((x_c, 1))$ *and* $\Gamma \in C^2((x_c, 1))$ *and which satisfies the boundary conditions (4.18)-(4.21) is real analytic in* $(x_c, 1)$*.*

Proof. If we set $H = F'$ and $\Delta = \Gamma'$ the system of equations (4.13)-(4.15) can be written as

$$\begin{aligned} \mathbf{y}' &= \mathbf{f}(x, \mathbf{y}), \text{ where} && (4.44) \\ \mathbf{y} &= [\psi, F, H, \Gamma, \Delta]^t, \text{ and} && (4.45) \\ \mathbf{f} &= \begin{bmatrix} \frac{-2x\psi + \psi^2/2 + F}{1-x^2} \\ H \\ \frac{-2xH + 2F + \Gamma^2}{1-x^2} \\ \Delta \\ \frac{\psi\Delta}{1-x^2} \end{bmatrix}. && (4.46) \end{aligned}$$

When ψ, F, H, Γ and Δ are all bounded, it is evident that $\mathbf{f}$ is an analytic function of x and $\mathbf{y}$ for all $x \neq \pm 1$. By assumption, this boundedness criterion is satisfied for $(x_c, 1)$, and hence by continuity in a neighbourhood of this line segment. Hence by Cauchy's existence theorem, locally there exists a unique analytic function in the vicinity of every point on $(x_c, 1)$. It has long been known that the solution obtain in this way is unique even in C^1, see for example [31] or [32], and therefore it must coincide with the solution we have assumed to exist. □

In Subsection 4.2.1 we required that a conically self-similar solution satisfies $\left|\psi'(1)\right| < \infty$. We will now show that this implies that all of $\psi'(1)$, $F''(1)$ and $\Gamma'(1)$ are finite for a conically self-similar solution.

Lemma 2 *Any solution to (4.13)-(4.15) such that* $\psi \in C^1((x_c, 1))$*,* $F \in C^2((x_c, 1))$ *and* $\Gamma \in C^2((x_c, 1))$ *and which satisfies the boundary conditions (4.18)-(4.21), which include the statement* $\left|\psi'(1)\right| < \infty$*, also satisfies the conditions* $\left|\Gamma'(1)\right| < \infty$ *and* $\left|F''(1)\right| < \infty$*.*

Proof. Formally, we can integrate (4.15) to obtain

$$\Gamma'(x) = \Gamma'(\tilde{x}) \exp\left(\int_{\tilde{x}}^{x} \frac{\psi(t)\, dt}{1-t^2}\right). \tag{4.47}$$

By assumption ψ is bounded and it satisfies $\psi = M(1-x) + o(1-x)$ near $x = 1$. Consequently, (4.47) is well defined, and the integral is finite for $x = 1$ and any $\tilde{x} \in (x_c, 1)$. However, by Lemma 1 we have that $\Gamma'(\tilde{x}) < \infty$ for any $\tilde{x} \in (x_c, 1)$, and therefore it follows that $\Gamma'(1) < \infty$. We have thus proved that for some N we have that

$$\Gamma = N(1-x) + o(1-x) \tag{4.48}$$

in the vicinity of $x = 1$.

Let $\tilde{x} \in (x_c, 1)$, (it can be allowed to be x_c, if $x_c \neq -1$). By the method of variable coefficients we can solve (4.14) to obtain

$$F(x) = -(1-x)^2 \int_{\tilde{x}}^{x} \frac{t\Gamma^2(t)\, dt}{(1-t^2)^2} - x \int_{x}^{1} \frac{\Gamma^2(t)\, dt}{(1+t)^2} - \frac{T^* \Gamma_c^2}{2} (1-x)^2 \ , \quad (4.49)$$

where the integrals are finite, since Γ is finite and satisfies (4.48). By twice differentiating this function we see that

$$F''(x) = -2 \int_{\tilde{x}}^{x} \frac{t\Gamma^2(t)\, dt}{(1-t^2)^2} + \frac{\Gamma^2(x)}{1-x^2} - \frac{T^* \Gamma_c^2}{2} \ . \quad (4.50)$$

By Lemma 1 we have that F is analytic in $(x_c, 1)$ and consequently T^* is finite. Furthermore, since Γ is finite and satisfies (4.48) we have that

$$\int_{\tilde{x}}^{1} \frac{t\Gamma^2(t)\, dt}{(1-t^2)^2} + \lim_{x \to 1^-} \frac{\Gamma^2(x)}{1-x^2} < \infty \ , \quad (4.51)$$

and this concludes the proof of the lemma. □

With this lemma we are now ready to prove that the singular system of ODE:s (4.13)-(4.15) with the conditions (4.18)-(4.19) at $x = 1$, admits an analytic solution in a disc in the complex plane around the singularity of the system at $x = 1$. For this proposition we will therefore let the independent variable be complex, and to emphasise this we will call it $\zeta \equiv x + iy$.

Proposition 1 *Consider the system*

$$\begin{aligned} \left(1-\zeta^2\right)\psi' + 2\zeta\psi - \frac{1}{2}\psi^2 &= F \ , \quad (4.52) \\ \left(1-\zeta^2\right)F'' + 2\zeta F' - 2F &= \Gamma^2 \ , \quad (4.53) \\ \left(1-\zeta^2\right)\Gamma'' &= \psi\Gamma' \ . \quad (4.54) \end{aligned}$$

with the conditions at $\zeta = 1$*:*

$$\psi(1) = \Gamma(1) = F(1) = F'(1) = 0 \ , \quad (4.55)$$

and let

$$M = \max\left\{ \left|\psi'(1)\right|, \frac{\left|F''(1)\right|}{2}, \left|\Gamma'(1)\right| \right\} \ . \quad (4.56)$$

Then there exist $\psi, \Gamma, F \in A\left(B\left(1, \frac{1}{kM}\right)\right)$ *which solve the system (4.52)-(4.54) with conditions (4.55). Furthermore we can choose* k *to be*

$$k = \frac{1 + \sqrt{M^2 + 4M + 1}}{4M} \ . \quad (4.57)$$

Remark 1: Notice k in (4.57) is a decreasing function of M, which gives us the following estimate for $M \geq 1$:

$$1 - \frac{4}{M} \leq 1 - \frac{1}{kM} \leq 1 - \frac{1}{M} \tag{4.58}$$

Remark 2: Notice that kM with k defined in (4.57) is an increasing function of M which gives us the following estimate for $M \leq 1$:

$$-1 \leq 1 - \frac{1}{kM} \leq 0 \tag{4.59}$$

Proof.
The idea of the proof is to set

$$\psi = \sum_{n \geq 0} p_n (1-\zeta)^n \tag{4.60}$$

$$F = \sum_{n \geq 0} f_n (1-\zeta)^n \tag{4.61}$$

$$\Gamma = \sum_{n \geq 0} g_n (1-\zeta)^n \quad , \tag{4.62}$$

and then to prove that

$$\limsup_{n \to \infty} \sqrt[n]{\max\left\{|p_n|, |f_n|, |g_n|\right\}} \leq kM \quad , \tag{4.63}$$

with k given by (4.57). Because then the proposition follows from basic analytic function theory.

Insertion of (4.60)-(4.62) into (4.52)-(4.54) yields the following equations

$$\begin{aligned} &\sum_{n \geq 0} p_n \left\{ (n-2)(1-\zeta)^{n+1} - 2(n-1)(1-\zeta)^n \right\} - \\ &- \frac{1}{2} \sum_{n \geq 0} \left(\sum_{i=0}^{n} p_i p_{n-i} \right) (1-\zeta)^n = \sum_{n \geq 0} f_n (1-\zeta)^n \end{aligned} \tag{4.64}$$

$$\begin{aligned} &\sum_{n \geq 0} f_n \left\{ 2n(n-2)(1-\zeta)^{n-1} - (n-1)(n-2)(1-\zeta)^n \right\} = \\ &= \sum_{n \geq 0} \left(\sum_{i=0}^{n} g_i g_{n-i} \right) (1-\zeta)^n \end{aligned} \tag{4.65}$$

$$\begin{aligned} &\sum_{n \geq 0} g_n n(n-1) \left\{ 2(1-\zeta)^{n-1} - (1-\zeta)^n \right\} = \\ &= \sum_{n \geq 0} \left(\sum_{i=0}^{n} (n+1-i) p_i g_{n+1-i} \right) (1-\zeta)^n \quad . \end{aligned} \tag{4.66}$$

If we identify coefficients in these equations we obtain the following system of non-linear recurrence equations

$$\begin{aligned}
2p_n &= \frac{n-3}{n-1}p_{n-1} - \frac{1}{2(n-1)}\sum_{i=0}^{n} p_i p_{n-i} - \frac{1}{n-1}f_n && (4.67)\\
2f_{n+1} &= \frac{n-2}{n+1}f_n + \frac{1}{(n+1)(n-1)}\sum_{i=0}^{n} g_i g_{n-i} && (4.68)\\
2g_n &= \frac{n-2}{n}g_{n-1} - \frac{1}{n(n-1)}\sum_{i=0}^{n}(n-i)\,p_i g_{n-i}\ , && (4.69)
\end{aligned}$$

for $n \geq 2$. The remaining five equations are

$$\begin{aligned}
2p_0 - \frac{1}{2}p_0^2 - f_0 &= 0 && (4.70)\\
2p_0 + p_0 p_1 + f_1 &= 0 && (4.71)\\
2f_0 + 2f_1 + g_0^2 &= 0 && (4.72)\\
2g_0 g_1 &= 0 && (4.73)\\
p_0 g_1 &= 0\ . && (4.74)
\end{aligned}$$

These equations show that an analytic solution to (4.52)-(4.54) with $\psi(1) = p_0 = 0$ must have the boundary conditions (4.55). These boundary conditions can also be expressed as

$$p_0 = f_0 = f_1 = g_0 = 0\ . \qquad (4.75)$$

As a consequence of these boundary conditions, we can choose p_1, f_2 and g_1 arbitrarily. From the definition of M in (4.56) we have that

$$M = \max\{|p_1|, |f_2|, |g_1|\}\ . \qquad (4.76)$$

If we now analogously define M_n for all $n \in \mathbb{Z}^+$,

$$M_n = \max\{|p_n|, |f_{n+1}|, |g_n|\}\ , \qquad (4.77)$$

we have the following lemma

Lemma 3 *The M_n's defined above are bounded by*

$$M_n \leq \gamma (kM)^n\ , \qquad (4.78)$$

where γ and k can be any positive numbers which satisfy

$$\begin{aligned}
\gamma k &\geq 1 && (4.79)\\
\gamma k^2 &\geq \frac{1}{4} + \frac{1}{M} && (4.80)\\
\frac{1}{2kM} + \frac{\gamma}{4} &\leq 1\ . && (4.81)
\end{aligned}$$

For any M, the smallest value of k is obtained when

$$\gamma = 4\frac{\left(\sqrt{M^2+4M+1}-1\right)^2}{M^2+4M} \quad (4.82)$$

$$k = \frac{\sqrt{M^2+4M+1}+1}{4M} . \quad (4.83)$$

Because of (4.63), Proposition 1 follows directly from this lemma. □

Proof. of Lemma 3
To prove Lemma 3 we will first assume that (4.79)-(4.81) hold and we will then use induction to show that this implies that (4.78) holds. Finally we will show that the smallest value of k which satisfy (4.79)-(4.81) is obtained with γ and k given by (4.82) and (4.83) respectively.

First we note that if (4.79) holds, then the lemma holds for $n = 1$.

If we use the conditions (4.75) the equations (4.67)-(4.69) reduce slightly to

$$p_n = \frac{(n-3)}{2(n-1)}p_{n-1} - \frac{1}{4(n-1)}\sum_{i=1}^{n-1} p_i p_{n-i} - \frac{1}{2(n-1)}f_n \quad (4.84)$$

$$f_{n+1} = \frac{(n-2)}{2(n+1)}f_n + \frac{1}{2(n^2-1)}\sum_{i=1}^{n-1} g_i g_{n-i} \quad (4.85)$$

$$g_n = \frac{(n-2)}{2n}g_{n-1} - \frac{1}{2n(n-1)}\sum_{i=1}^{n-1}(n-i)\,p_i g_{n-i} . \quad (4.86)$$

For $n = 2$ (4.84)-(4.86) imply that

$$|p_2| \le M + \frac{M^2}{4} \quad (4.87)$$

$$|f_2| \le \frac{M^2}{6} \quad (4.88)$$

$$|g_2| \le \frac{M^2}{4} , \quad (4.89)$$

and consequently $M_2 \le M + \frac{M^2}{4}$, which implies that the lemma holds for $n = 2$ if

$$\gamma k^2 \ge \frac{1}{4} + \frac{1}{M} \quad (4.90)$$

which we have assumed to be true (4.80).

To prove the lemma for $n \ge 3$ we will use induction in n. Let us now assume that Lemma 3 holds for $n = 1, 2, \ldots, m-1$. We will prove that this implies the lemma for $n = m$.

If $m \geq 3$ we can obtain the following estimates from (4.84)-(4.86).

$$\begin{aligned} |p_m| &\leq \frac{1}{2}M_{m-1} + \frac{1}{4(m-1)}\sum_{i=1}^{m-1} M_i M_{m-i} && (4.91) \\ |f_{m+1}| &\leq \frac{1}{2}M_{m-1} + \frac{1}{2(m^2-1)}\sum_{i=1}^{m-1} M_i M_{m-i} && (4.92) \\ |g_m| &\leq \frac{1}{2}M_{m-1} + \frac{1}{2m(m-1)}\sum_{i=1}^{m-1} (m-i) M_i M_{m-i} . && (4.93) \end{aligned}$$

We immediately find that the right hand side in (4.92) is bounded by that in (4.91) and thus we have the following estimate for M_m:

$$M_m \leq \frac{M_{m-1}}{2} + \frac{\max\left\{\frac{1}{2}\sum_{i=1}^{m-1} M_i M_{m-i}, \frac{1}{m}\sum_{i=1}^{m-1}(m-i) M_i M_{m-i}\right\}}{2(m-1)} \qquad (4.94)$$

We can now use the induction hypotheses in (4.91) and (4.93) to obtain

$$\begin{aligned} |p_m| &\leq \gamma (kM)^m \left(\frac{1}{2kM} + \frac{\gamma}{4(m-1)}\sum_{1}^{m-1} 1\right) && (4.95) \\ &= \gamma (kM)^n \left(\frac{1}{2kM} + \frac{\gamma}{4}\right) && (4.96) \\ &\leq \gamma (kM)^n && (4.97) \\ |g_m| &\leq \gamma (kM)^m \left(\frac{1}{2kM} + \frac{\gamma}{2m(m-1)}\sum_{1}^{m-1} (m-i)\right) && (4.98) \\ &= \gamma (kM)^n \left(\frac{1}{2kM} + \frac{\gamma}{4}\right) && (4.99) \\ &\leq \gamma (kM)^n && (4.100) \end{aligned}$$

where we have used (4.81) and the basic result

$$\sum_{i=1}^{m-1}(m-i) = \sum_{i=1}^{m-1} i = \frac{m(m-1)}{2} . \qquad (4.101)$$

Under the assumption that (4.79)-(4.81) hold, we have now proved that $M_n \leq \gamma (kM)^n$.

To finish the proof of the lemma we must only find the minimum value of k such that

$$\begin{aligned} \gamma k &\geq 1 && (4.102) \\ \gamma k^2 &\geq \frac{1}{4} + \frac{1}{M} && (4.103) \\ \frac{1}{2kM} + \frac{\gamma}{4} &\leq 1 && (4.104) \end{aligned}$$

are satisfied, and $k > 0, \gamma > 0$. First of all notice that, all of the conditions (4.102)-(4.104) have the property that if they are satisfied for $(\gamma^\star, k^\star)$ then they are satisfied for $(\gamma^\star, k)$ for all $k \geq k^\star$. Each of the conditions therefore require us to be above a curve in the $\gamma - k$ plane.

Now notice that the curves

$$\begin{aligned} \gamma k &= 1 & (4.105) \\ \gamma k^2 &= \frac{1}{4} + \frac{1}{M} & (4.106) \end{aligned}$$

intersect when $k^\dagger = \frac{M+4}{4M}$ and $\gamma^\dagger = \frac{4M}{M+4}$. Therefore both of the conditions (4.102) and (4.103) are satisfied if and only if

$$\begin{cases} \gamma k \geq 1, \text{ for } \gamma \leq \gamma^\dagger \\ \gamma k^2 \geq \frac{1}{4} + \frac{1}{M}, \text{ for } \gamma \geq \gamma^\dagger \end{cases} \tag{4.107}$$

For both of (4.102) and (4.103) it is clear that k decreases with increasing γ, but for (4.104) we have the opposite situation. Consequently, we can say that either we have the situation in figure 4.1 (a) or the one in figure 4.1 (b). In both these figures, the minimum k is obtained when

$$\frac{1}{2kM} + \frac{\gamma}{4} = 1 \tag{4.108}$$

intersects the boundary of the region defined by (4.107). We will find this point by finding the point of intersection between the curves defined by (4.106) and (4.108) and prove that for this point of intersection $\gamma k \geq 1$, which shows that $\gamma \geq \gamma^\dagger$

To find the point of intersection between the curves defined by (4.106) and (4.108) notice first that the latter equation implies that

$$\gamma = 4 - \frac{2}{Mk} . \tag{4.109}$$

Substitution into (4.103) yields

$$k^2 - \frac{k}{2M} - \frac{1}{16} - \frac{1}{4M} = 0 , \tag{4.110}$$

which has exactly one positive root given by

$$k^* = \frac{\sqrt{M^2 + 4M + 1} + 1}{4M} . \tag{4.111}$$

Backsubstitution into (4.109) gives after simplification

$$\gamma^* = 4\frac{\left(\sqrt{M^2 + 4M + 1} - 1\right)^2}{M^2 + 4M} . \tag{4.112}$$

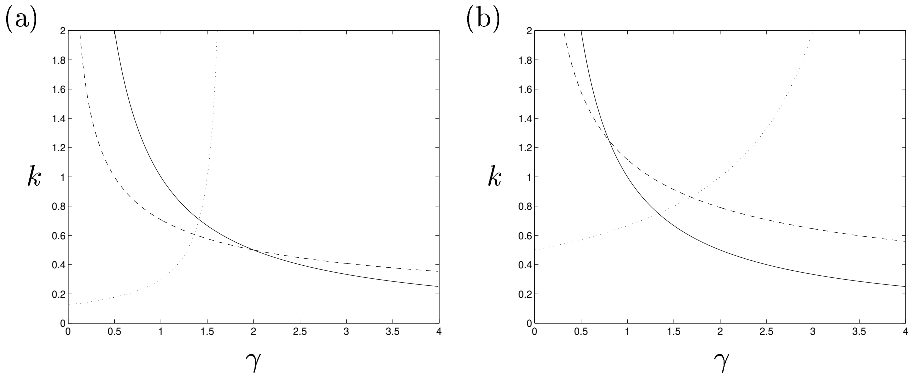

Figure 4.1: These curves illustrate typical boundaries of the regions in the $\gamma - k$ plane where each of the conditions (4.102)-(4.104) hold. To satisfy all these conditions we must be above all the three curves in the diagrams. In these figures the solid curves are typical instances of (4.105), the dashed curves illustrate (4.106) and the dotted curves show (4.108).The figure illustrates how (4.108) can intersect the boundary of the region defined by (4.107). The two illustrated cases are the only ones which can occur, and from the pictures it is clear that for (a) we have that (4.108) intersect the boundary of (4.107) when $\gamma < \gamma^\dagger$ and that for (b) this point of intersection occurs when $\gamma > \gamma^\dagger$.

These values satisfy (4.102) since

$$k^*\gamma^* = \frac{\sqrt{M^2+4M+1}-1}{M} \geq \frac{M+1-1}{M} = 1 \ , \tag{4.113}$$

and therefore we have seen that in fact only the case in figure 4.1(b) occurs.

This concludes the proof of the lemma. □

We must now establish that the analytic solution around $x = 1$ provided by Proposition 1 is the only solution in C^1 as well. Indeed, we will prove the following proposition:

Proposition 2 *Let $\tilde{x}$ be arbitrary, $I = (1-\tilde{x}, 1+\tilde{x})$, $\psi \in C^1(I)$, $F \in C^2(I)$ and $\Gamma \in C^2(I)$ be a solution to (4.13)-(4.15), which satisfies the conditions (4.18)-(4.19). Let furthermore $\psi'(1) = \tilde{A}$, $\Gamma'(1) = B$ and $F''(1) = P$, then this solution is uniquely determined by $\tilde{A}$, B and P.*

Remark: This proposition is really enough to justify the use of the numerical method mentioned in the beginning of this section.

Proof. We now make the substitutions $\xi = \frac{\psi}{1-x^2}$ and $\Delta = \Gamma'$. This implies that $\Delta(1) = \Gamma'(1) = B$ and by l'Hôpital's rule we have that $\xi(1) = -\frac{\psi'(1)}{2} = -\frac{\tilde{A}}{2} \equiv A$.

By using the method of variable coefficients we can once again solve (4.14) to obtain the slightly different formula

$$F(x) = (1-x)^2 \int_x^1 \frac{t\Gamma^2(t)\,dt}{(1-t^2)^2} - x\int_x^1 \frac{\Gamma^2(t)\,dt}{(1+t)^2} - \frac{S\Gamma_c^2}{2}(1-x)^2 \ , \qquad (4.114)$$

where once again the integrals are finite since Γ is finite and satisfies (4.48). By twice differentiating this function we see that

$$F''(x) = 2\int_x^1 \frac{t\Gamma^2(t)\,dt}{(1-t^2)^2} + \frac{\Gamma^2(x)}{1-x^2} - \frac{S\Gamma_c^2}{2} \ . \qquad (4.115)$$

From this equation we see that $F''(1) = -\frac{S\Gamma_c^2}{2} = P$, and thus we can replace P by S in subsequent argument.

Furthermore, by the Fundamental Theorem of Calculus, Γ satisfies

$$\Gamma(x) = -\int_x^1 \Delta(t)\,dt \ , \qquad (4.116)$$

and therefore we can reduce (4.13)-(4.15) to

$$\begin{aligned} \xi' &= \frac{1}{2}\xi^2 + \frac{G(x,\Delta)}{(1+x)^2} & (4.117)\\ \Delta' &= \xi\Delta, & (4.118) \end{aligned}$$

where

$$\begin{aligned} G(x,\Delta) &= \int_x^1 \frac{t\Gamma^2(t,\Delta)\,dt}{(1-t^2)^2} - \\ &- \frac{x}{(1-x)^2}\int_x^1 \frac{\Gamma^2(t,\Delta)\,dt}{(1+t)^2} - \frac{S\Gamma_c^2}{2} \text{ and} & (4.119)\\ \Gamma(x,\Delta) &= -\int_x^1 \Delta(t)\,dt \ . & (4.120) \end{aligned}$$

Our system (4.117)-(4.118) is thus on the form

$$\begin{aligned} \mathbf{y}' &= \mathbf{f}(x,\mathbf{y}) \ , \text{ where} & (4.121)\\ \mathbf{y} &= [\xi,\Delta]^t & (4.122)\\ \mathbf{f} &= [f_1,f_2]^t \ . & (4.123) \end{aligned}$$

From now on let us fix S at an arbitrary value, and we consider the region:

$$\begin{aligned} A-s &\leq \xi \leq A+s & (4.124)\\ B-s &\leq \Delta \leq B+s & (4.125)\\ 1-\varepsilon &\leq x \leq 1+\varepsilon, & (4.126) \end{aligned}$$

where $s > 0$ and $\varepsilon > 0$.

For f_2 we now have the following Lipschitz estimate

$$\begin{aligned} |f_2(x,\mathbf{y}) - f_2(x,\mathbf{Y})| &\leq |\xi|\,|\Delta-\delta| + |\delta|\,|\xi-\Xi| && (4.127)\\ &\leq (|A|+|B|+2s)\,|\mathbf{y}-\mathbf{Y}| \ . && (4.128)\end{aligned}$$

To prove a similar estimate for f_1 we need the following estimates, which are immediate consequences of (4.120)

$$\begin{aligned} |\Gamma(x,\Delta)| &\leq (1-x)\,(|B|+s) && (4.129)\\ |\Gamma(x,\Delta)-\Gamma(x,\delta)| &\leq (1-x)\,|\Delta-\delta| \ . && (4.130)\end{aligned}$$

If we use these relations and (4.119) we can make the following estimates

$$\begin{aligned} &|G(x,\Delta)-G(x,\delta)| \leq && (4.131)\\ &\leq (|B|+s)\,|\Delta-\delta| \left\{ \int_x^1 \frac{|t|\,dt}{(1+t)^2} + \frac{|x|}{(1-x)^2}\int_x^1 \frac{(1-t)^2\,dt}{(1+t)^2} \right\} && (4.132)\\ &= (|B|+s)\,|\Delta-\delta| \left\{ v(x) + \frac{x}{(1-x)^2} w(x) \right\} \ , && (4.133)\end{aligned}$$

where

$$\begin{aligned} v(x) &= \begin{cases} \frac{x-1}{2(x+1)} + \ln 2 - \ln|1+x|, & \text{for } x \geq 0 \\ \frac{-1-3x}{2(x+1)} + \ln 2 + \ln|1+x|, & \text{for } x < 0 \end{cases} \text{, and} && (4.134)\\ w(x) &= \int_x^1 \frac{(1-t)^2}{(1+t)^2} dt = -x - 1 + \frac{4}{1+x} + 4\ln\frac{|1+x|}{2} \ . && (4.135)\end{aligned}$$

Therefore, we have that

$$|G(x,\Delta)-G(x,\delta)| \leq C\,(|B|+s)\,|\Delta-\delta| \ , \qquad (4.136)$$

if we only can prove that $w(x) = \mathcal{O}\left((1-x)^2\right)$, and to do this it suffices to prove that $w(1) = w^{'}(1) = 0$. However, from (4.135) we see that $w(1) = 0$. Differentiation yields

$$w^{'}(x) = -1 - \frac{4}{(1+x)^2} + \frac{4}{(1+x)} \qquad (4.137)$$

and from this relation we find that $w^{'}(1) = 0$, and thus $w = \mathcal{O}\left((1-x)^2\right)$, which implies (4.136).

Now we can obtain a Lipschitz estimate for f_1

$$\begin{aligned} &|f_1(x,\mathbf{y}) - f_1(x,\mathbf{Y})| \leq && (4.138)\\ &\leq (|A|+s)\,|\xi-\Xi| + \frac{|G(x,\Delta)-G(x,\delta)|}{(1+x)^2} && (4.139)\\ &\leq (|A|+s)\,|\xi-\Xi| + \frac{C}{(2-|\varepsilon|)^2}(|B|+s)\,|\Delta-\delta| && (4.140)\\ &\leq \left\{ |A| + s + \frac{C}{(2-|\varepsilon|)^2}(|B|+s) \right\} |\mathbf{y}-\mathbf{Y}| \ . && (4.141)\end{aligned}$$

Taken together (4.128) and (4.141) imply that

$$|\mathbf{f}(x,\mathbf{y}) - \mathbf{f}(x,\mathbf{Y})| \leq L\,|\mathbf{y} - \mathbf{Y}| \ , \tag{4.142}$$

for some finite constant L. By standard ODE theory this implies that there exists a unique C^1 solution to (4.117)-(4.118) which passes through $\xi(1) = A$ and $\Delta(1) = B$. Recall that S is arbitrary, and therefore the proposition follows. □

Taken together Lemma 1, Lemma 2, Proposition 1 and Proposition 2 imply Theorem 3.

The result in this section indicate that the singularity at $x = 1$ is only apparent. Possibly, the proof of Theorem 3 can be greatly simplified by a change of variables at an earlier stage of the argument.

4.5 On the existence and regularity of a second order non-swirling correction term to conically self-similar solutions

In this subsection we will study the question of existence and regularity of a solution to (4.17), under the assumption that there exists a solution to (4.13)-(4.15), such that $\psi \in C^1((x_c,1])$, $F \in C^2((x_c,1])$ and $\Gamma \in C^2((x_c,1])$, which also satisfies the boundary conditions (4.18)-(4.21) and has the prescribed value of J_z. According to Theorem 3 we have that such a solution is real analytic in $(x_c,1)$ and analytic in some disc of the complex plane, $B(1,r)$, $r > 0$. In fact, in this section we will prove the following apparently new result:

Theorem 4 *Assume that ψ is as described in the previous paragraph and let N be any neighbourhood around $x = 1$, then for any α there exists a $z^{'} \in C^{\omega}((x_c,1])$, unique in the class $C^2((x_c,1]) \cap C^{\omega}(N)$, which is a solution to*

$$\left(1 - x^2\right) z^{'''} - 2xz^{''} - \psi z^{''} - 3\psi^{'} z^{'} + 6z^{'} = 3c \ . \tag{4.143}$$

with the initial condition $z^{'}(1) = \alpha$. Here we have used C^{ω} to denote the class of real analytic functions.

Remark 1: If $x_c = -1$ we can have that $\lim_{x\to-1^+} z^{'}(x) = \pm\infty$. This comes as no real surprise since it is known [5] that $\psi^{'} = \frac{\Gamma_c^2}{4(1+x)} + \mathcal{O}(1)$ in the vicinity of $x = -1$.

Remark 2: The cases when $c \neq 0$ is of questionable importance. Indeed in [17] it is shown that if $\Gamma \equiv 0$ and $x_c = -1$ then there does not exist a regular $z^{'}$ which satisfies (4.17) for any $c \neq 0$. Towards the end of the chapter we will see that if $x_c = -1$ then possible solutions to (4.17) with $c \neq 0$ have undesirable physical properties even for non-vanishing Γ. For $x_c \neq -1$ the picture is not as clear, but we will nonetheless concentrate on the case $c = 0$. Thus, it should be stressed that if $z_1^{'}$ is a solution to (4.17) with $c = 0$ then so is $kz_1^{'}$ for any constant k.

The main step in the proof of this theorem is the following lemma.

Lemma 4 *Let ψ be part of the assumed conically self-similar solution. From Theorem 3 we know that it is analytic in some disc around $x = 1$. Then for some $r > 0$ there exists a unique $z \in A(B(1,r))$ which solves (4.143) with $z^{'}(1) = \alpha$, $z(1) = \beta$ for any α, β and c.*

Proof. of Theorem 4
We set $y = z^{'}$ and write (4.143) as

$$y^{''} - \frac{2x + \psi}{1 - x^2}y^{'} + \frac{6 - 3\psi^{'}}{1 - x^2}y = \frac{3c}{1 - x^2} \ . \tag{4.144}$$

This equation is linear in y and the only singularities are at $x = \pm 1$ and at any singularities of ψ. We know that ψ has no singularities in some open domain containing $(x_c, 1)$. Therefore by a variant of Cauchy's existence theorem (see for example [32]) there exists a real analytic solution for every $x \in (x_c, 1)$, which has a positive radius of convergence. Therefore we can at least extend any such solution to solution analytic in $(x_c, 1)$. It is also known that this solution is unique in C^2, see for example [32] and [31].

Consequently, the solution obtained from Lemma 4 is analytic in $(x_c, 1]$, and it is unique in the class $C^2((x_c, 1)) \cap C^{\omega}(N)$, where N is some neighbourhood of $x = 1$. This concludes the proof of the theorem. □

Proof. of Lemma 4
We will only prove this lemma for the case $c = 0$. For the general case we have verified that the same method of proof works as for Proposition 1, but since it contains no new ideas we leave it to the interested reader.

For $c = 0$, which is the most important case, we will instead present a much shorter proof, based on the linearity of (4.143), which allows us to use the theory for ordinary differential equations with coefficients outside some regular singularities. This theory is presented in for example [32], [33] and [34].

Let us now set $w = z^{'}$ and rewrite (4.17) as

$$w^{''} + \frac{2\zeta + \psi}{(\zeta + 1)(\zeta - 1)}w^{'} + \frac{3\psi^{'} - 6}{(\zeta + 1)(\zeta - 1)}w = 0 \ . \tag{4.145}$$

By assumption we know that $\psi \in A(1, r)$ for some $r > 0$, and in addition we know that $\psi(1) = 0$. Consequently, close to $\zeta = 1$, (4.145) is on the form

$$y^{''}(\zeta) + p(\zeta)\, y^{'}(\zeta) + q(\zeta)\, y(\zeta) = 0 \ , \tag{4.146}$$

where

$$p(\zeta) = \frac{p_0}{\zeta} + p_1 + p_2\zeta + \dots \text{ , and} \tag{4.147}$$

$$q(\zeta) = \frac{q_0}{\zeta^2} + \frac{q_1}{\zeta} + q_2 + q_3\zeta + \dots \text{ .} \tag{4.148}$$

A second order ordinary differential equation on this form is called regularly singular if p and q are analytic in a neighbourhood of the origin.

For a regularly singular second order ordinary differential equation the form of the solutions is determined by the solutions to the indicial equation

$$I(\mu) = \mu(\mu - 1) + p_0\mu + q_0 = 0 \text{ .} \tag{4.149}$$

In the case of (4.145) we have that $p_0 = 1$ and $q_0 = 0$ and thus the indicial equation becomes

$$I(\mu) = \mu^2 = 0 \text{ .} \tag{4.150}$$

Since the indicial equation has a double root at zero, the theory for regularly singular second order differential equations (Frobenius' method) [32], [33] or [34], tell us that in a neighbourhood of $\zeta = 1$ the solution to (4.145) is given by

$$w(\zeta) = k_1 a(\zeta) + k_2 \left\{\ln(\zeta - 1) a(\zeta) + (\zeta - 1)^n b(\zeta)\right\} \text{ ,} \tag{4.151}$$

where $\Re\nu \geq 0$, $a,\ b \in A(B(1,r))$ for some $r > 0$ and $a(1) \neq 0$. Naturally, we take such a branch of the logarithm function that is well-defined in a neighbourhood of the negative real axis.

Furthermore, the condition $w(1) = z'(1) = \alpha$ implies that $k_2 = 0$, since $|\ln(\zeta - 1)| \to \infty$ as $z \to 1^-$. Consequently, k_1 is uniquely determined by $z'(1)$. To summarise, we have shown that if $c = 0$ there exists a unique function $z(\zeta) \in A(B(1,r))$ such that $z' = k_1 a(z)$ is a solution to (4.143), and $z'(1) = \alpha$. $\square$

The regularity of the solution offered by Theorem 4 immediately yields the following refinement of Theorem 1

Corollary 1 *Let z' be a solution to (4.17) as in Theorem 4 and let $\psi \in C^\omega((x_c, 1))$ be part of a solution to (4.13)-(4.15), which satisfies $\psi(x_c) = \psi(1) = 0$.*
(a) If $x_c \neq 1$ then

$$J_2 = -x_c\left(1 - x_c^2\right) z''(x_c) - \left(1 - x_c^2\right) c \text{ ,} \tag{4.152}$$

(b) If $x_c = -1$ then

$$J_{2,0} = -c \text{ ,} \tag{4.153}$$

From Corollary 1 we find that $J_{2,0} = 0$ if and only if $c = 0$. As already mentioned, the case in (b) is a generalisation of Long's problem, which was considered by Burggraf and Foster, when they for physical reasons made their claim that $J_{2,0} = 0$. We have thus showed that this claim is correct if and only if $c = 0$. Furthermore, because of this result one can also question the relevance of the cases $x_c = -1$, $c \neq 0$, for the case of swirling conically self-similar solutions as well. Remember, that for the non-swirling conically self-similar solutions it is known [17] that no solution exists to (4.17) if $x_c = -1$, and $c \neq 0$.

It may also be noted, however, that Corollary 1 does not ensure that $J_2 = 0$ for general x_c. Of course, there is still the possibility that $z''(x_c) = 0$, but numerical computations suggest that this rarely, if ever, happens for non-trivial solutions to (4.17).

4.6 Numerical computation of conically self-similar solutions and the second-order non-swirling correction term

In the introduction we mentioned that there are three kinds of conically self-similar solutions to the Navier-Stokes equations.

- A near-axis jet. The fluid flows downstream in the vicinity of the symmetry axis, $x = 1$, and upstream close to the cone $x = x_c$.

- A surface jet. The fluid flows downstream along the cone $x = x_c$ and upstream along the symmetry axis.

- A two-cell flow. The fluid flows downstream along some cone $x = x_s$ and upstream both along the cone $x = x_c$ and along the symmetry axis.

Theoretical studies by for example Yih *et al* [24] show that these are the only possibilities. All three kinds of solutions have been obtained numerically, for example by Shtern and Hussain [27] and [5]. A feature of these numerical solutions is the existence of boundary layers near x_c, x_s and 1, and relatively slow variation elsewhere. This feature is increasingly pronounced as Γ_c and J_z increase. Even for moderate values of Γ_c this behaviour is consistent with the asymptotic analysis of the solutions presented in Shtern and Hussain [27] and [5]. In this section we will numerically seek conically self-similar solutions of the first and the last kind.

4.6.1 The numerical method for finding conically self-similar solutions to the Navier-Stokes equations

To find the second order non-swirling correction term numerically we first seeked a solution to (4.13)-(4.15) which satisfied the conditions (4.18)-(4.21) for a given Γ_c and then afterwards we solved (4.17) numerically with c=0, for some value of $z^{'}(1)$. It should be emphasised that it is simple to solve (4.17) once ψ is known, and it can for example be done by an ordinary Runge-Kutta method. The difficult part of the numerical solution therefore lies in solving (4.13)-(4.15) with the boundary conditions (4.18)-(4.21) for a given Γ_c. To do this we used a method of Shtern and Hussain [5] and [27]. If $x_s \neq 1$ we started by setting $\psi(x_s) = 0$ and guessing the values of $\Gamma(x_s)$, $\Gamma^{'}(x_s)$, $F(x_s)$ and $F^{'}(x_s)$. We then used a Runge-Kutta method to solve (4.13)-(4.15) in both directions starting from x_s. Afterwards we used a shooting method to adjust the values of $\Gamma(x_s)$, $\Gamma^{'}(x_s)$, $F(x_s)$ and $F^{'}(x_s)$, in order to satisfy $\psi(1) = \psi(x_c) = 0$, $\Gamma(1) = 0$ and $\Gamma(x_c) = \Gamma_c$. When this had been achieved we calculated the value of J_z. It should be stressed that in our numerical calculations we used x_s and not J_z as a controlling parameter.

To achieve good spatial resolution we used Chebyshev grids in each of the intervals $x_c \leq x \leq x_s$ and $x_s \leq x \leq 1$, which give us a high density of grid points in the boundary layers near x_c, x_s and 1. Normally we used 400 grid points, but some calculations were performed with 200 grid points, and the solutions coincided to three decimal places.

For the shooting method we used a modified Newton's method, where difference quotients were used to approximate the Jacobian, and to determine the length of the step in the direction of the gradient a line search was used.

When $x_s = 1$ we used a slightly different method. This time we choose, once again following Shtern and Hussain [27], some tentative values of $\psi^{'}(1)$, $\Gamma^{'}(1)$ and $F^{''}(1)$. With these values we computed $\Gamma^{''}(1) = -\frac{1}{2}\Gamma^{'}(1)\psi^{'}(1)$. Subsequently, we used a Runge-Kutta method to solve (4.13)-(4.15), and finally we used the shooting method outlined above to adjust the tentative values to satisfy (4.21) for the given value of Γ_c, and in addition, we this time adjusted our tentative values to give us a prescribed value of J_z.

4.6.2 The numerical results

We will begin by studying two-cell flows, and first of all we will study the changes in the conically self-similar solutions as Γ_c increases. In figure 4.2 we see that the absolute levels of ψ, $\psi^{'}$ and Γ are proportional to Γ_c whereas the absolute level of $z^{'}$ is proportional to Γ_c^4 if $z^{'}(1)$ is left unchanged. The most striking feature, however, is that all gradient get steeper, *i.e.* the boundary layers are increasingly dominant, as Γ_c increases. It is also apparent that as $\Gamma_c \to \infty$ the conically self-similar solutions approach the asymptotic solutions found in [5].

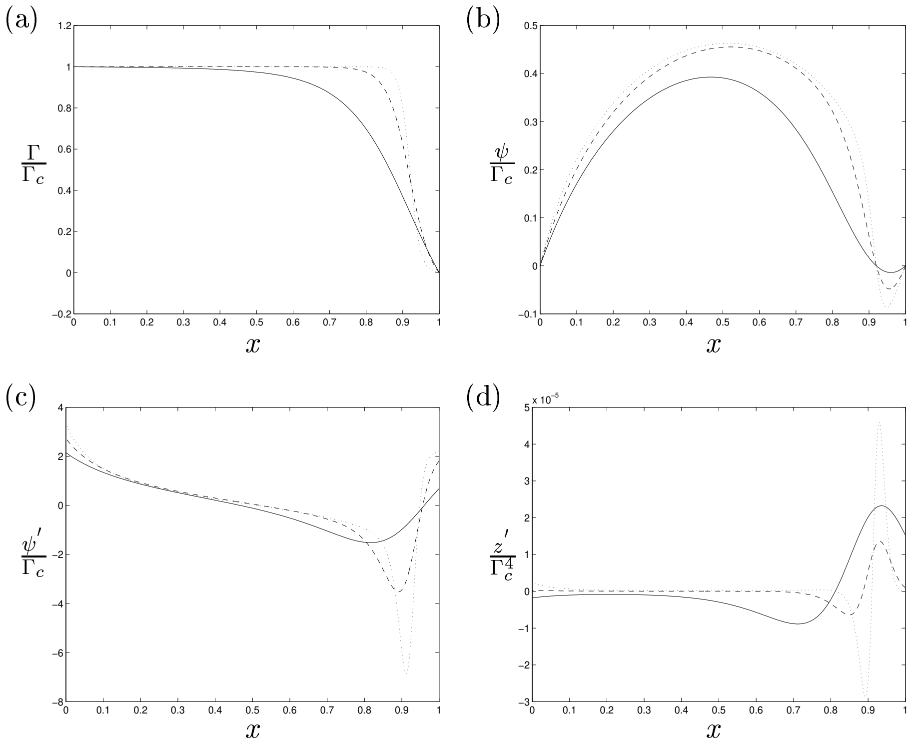

Figure 4.2: The development of the circulation function Γ (a), the first order streamfunction term ψ (b), its derivative $\psi^{'}$ (c) and the second order non-swirling correction term $z^{'}$ (d) for different values of Γ_c. For all the curves we had $x_c = 0$ and $x_s = 0.92$. The solid line shows the case when $\Gamma_c = 16$, the dashed line the one with $\Gamma_c = 32$ and the dotted line the one with $\Gamma_c = 64$.

We now turn our attention to how conically self-similar solutions are affected by changes in x_c and in x_s. In figure 4.3 ψ and Γ are presented for some combinations of values of x_c and x_s. We see that the steepest gradients of ψ and Γ occur, as expected, in the vicinity of x_s, wherever that happens to be. We also see that reducing the distance $x_s - x_c$ has a smoothing effect similar to that of decreasing Γ_c. In figure 4.4 we show the corresponding profiles of $\psi^{'}$ and $z^{'}$. As expected, we have a minimum of $\psi^{'}$ in the vicinity of x_s, but we can also make some other noteworthy observations. Firstly, we notice that in all cases, the effect of adding a second-order non-swirling correction term, is to move the azimuthal position of the maximum radial velocity in the vicinity of the apex of the cone. It appears to be moved outwards if $z^{'}(1) > 0$ and inwards if $z^{'}(1) < 0$. Secondly, we see from figure

4.4 that if $x_c = -1$ then both ψ' and z' approach infinity as $x \to -1^+$, but when $x_c = 0$ they are both bounded at x_c. Note that this is consistent with Remark 1 after Theorem 4.

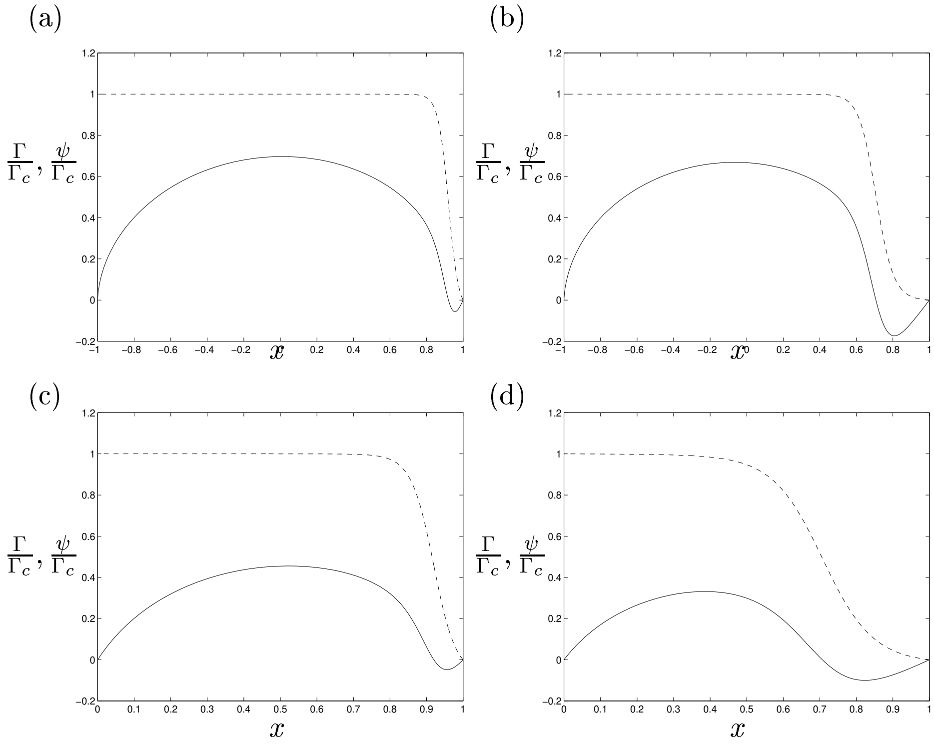

Figure 4.3: The solid lines show the distribution of the circulation function Γ, and the dashed lines show the distribution of the first order streamfunction term ψ. In all the figures $\Gamma_c = 32$, in (a) and (b) $x_c = -1$ and in (c) and (d) $x_c = 0$. In (a) and (c) $x_s = 0.92$ and in (b) and (d) $x_s = \frac{1}{\sqrt{2}}$.

To conclude the chapter we will briefly discuss the behaviour of the conically self-similar near-axis jets. We will restrict ourselves to the case $x_c = -1$, i.e. to the generalisation of Long's problem. In figure 4.5 we see the distributions of ψ and Γ for $M = 3.833$ and $M = 5.026$. The first value of M is just above the critical value $M_* \approx 3.742$, below which no conically self-similar near axis jet solutions can exist. From the distributions of ψ and Γ, it is difficult to tell the difference between these two cases. However, in figure 4.6 we show the corresponding profiles of ψ' and z', and when we magnify the region close to the symmetry axis, we notice that for $M = 5.026$ the maximum of ψ' is obtained on the symmetry axis, whereas when $M = 3.833$ the maximum axial velocity is obtained on a cone close to the symmetry axis.

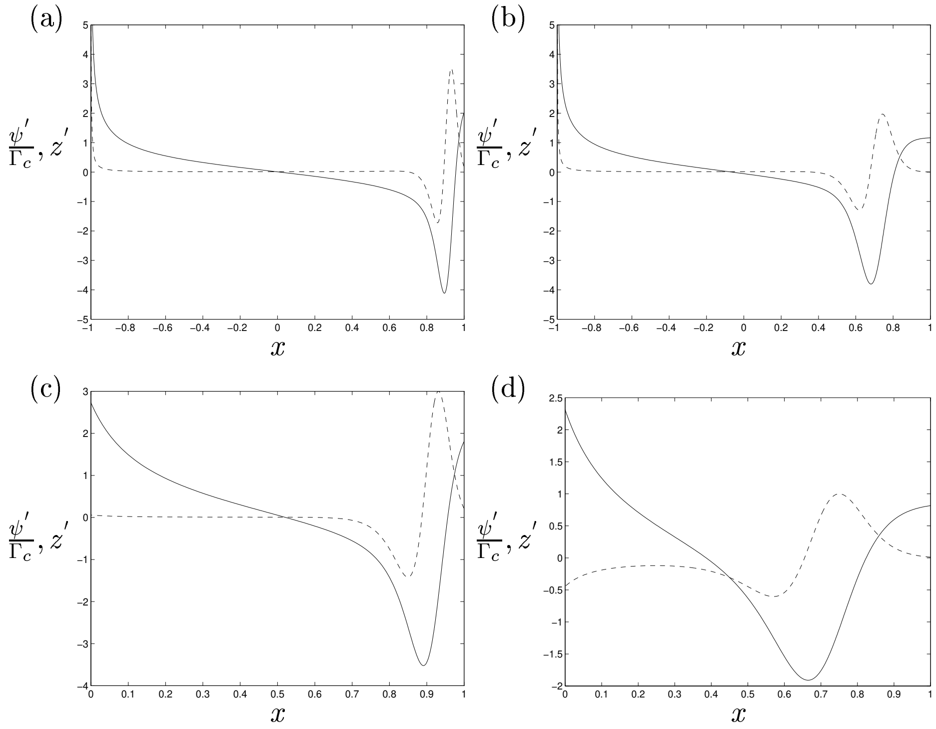

Figure 4.4: The solid lines show the derivative of the distribution of the first order streamfunction term ψ', and the dashed lines show the derivative of the distribution of the second order streamfunction term z'. In all the figures $\Gamma_c = 32$, in (a) and (b) $x_c = -1$ and in (c) and (d) $x_c = 0$. In (a) and (c) $x_s = 0.92$ and in (b) and (d) $x_s = \frac{1}{\sqrt{2}}$. In the different figures different values of $z'(1)$ have chosen to obtain curves of equal order of magnitude.

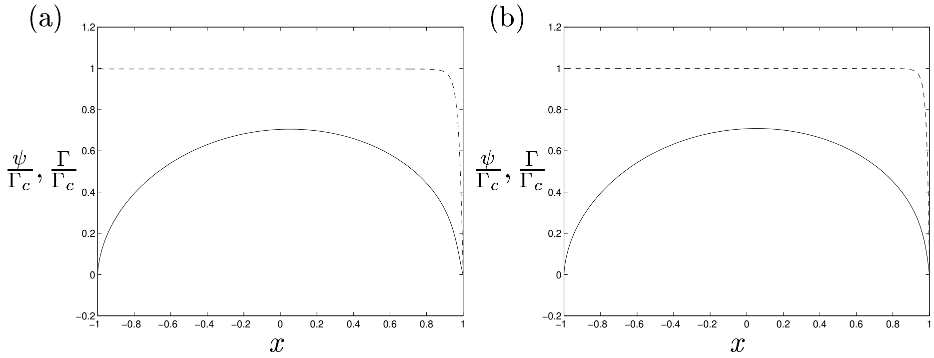

Figure 4.5: The solid lines show the distribution of the circulation function Γ, and the dashed lines show the distribution of the first order streamfunction term ψ for a near axis jet. In all the figures $x_c = -1$ and $x_s = 1$, in (a) $M = \frac{J_z}{\rho \nu^2 \Gamma_c^2} = 3.833$ and in (b) $M = \frac{J_z}{\rho \nu^2 \Gamma_c^2} = 5.026$.

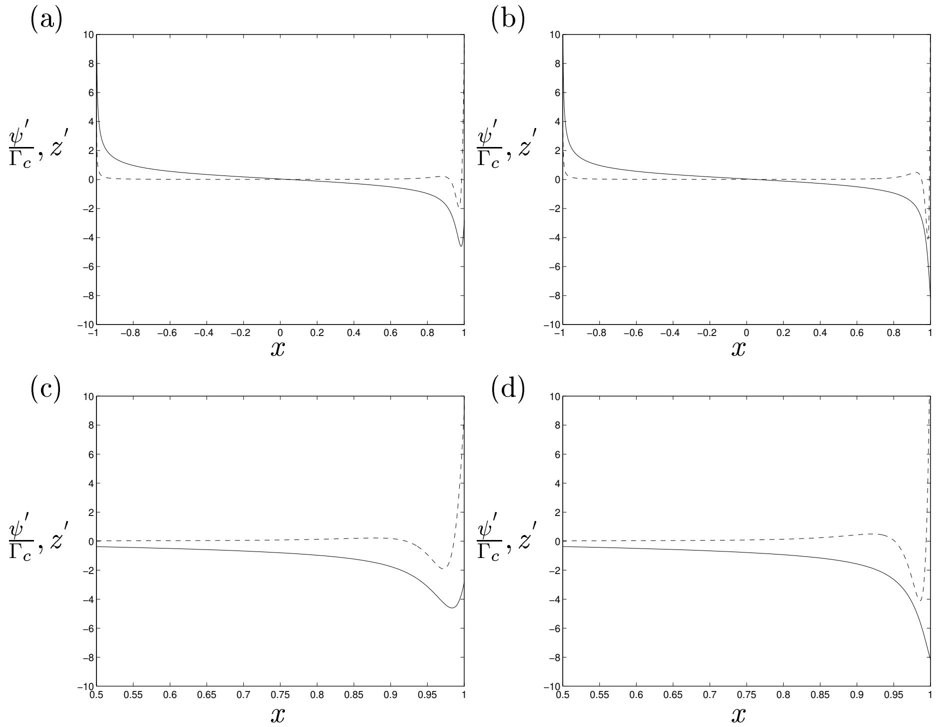

Figure 4.6: The solid lines show the derivative of the distribution of the first order streamfunction term $\psi^{'}$, and the dashed lines show the derivative of the distribution of the second order streamfunction term $z^{'}$ for a near axis jet. In all the figures $x_c = -1$ and $x_s = 1$, in (a) $M = \frac{J_0}{\rho\nu^2\Gamma_c^2} = 3.833$ and in (b) $M = \frac{J_0}{\rho\nu^2\Gamma_c^2} = 5.0265$. (c) and (d) are magnifications of the near axis regions of (a) and (b) respectively. In the all the figures $z^{'}(1) = 30$, which was chosen to obtain curves of equal order of magnitude.

Chapter 5

On the applicability of conical self-similarity to the understanding of combustion chamber flows

5.1 Introduction

In Chapter 3 we saw that the parameter M behaved comparatively well when the inlet geometry was changed (see table 3.1). This parameter M is omnipresent in the theory of conically self-similar solutions to the Navier-Stokes equation. In fact, Long [4] showed that his solutions, which are closely related to the near-axis jet solution with $x_c = -1$ discussed in Section 4.6.1, can only exist if $M > M_*$, where M_* is some constant. The best approximation of $M_* \approx 3.742$ is due to Burggraf and Foster [28]. One of the main results in Shtern and Hussain [5] is that for given x_c and Γ_c (which is used as a Reynolds number), there are values M_0, M_1 such that for $M_0 < M < M_*$ there exist conically self-similar solutions to the Navier-Stokes equations of the two-cell kind, but no near-axis jet ones. For $M > M_1$ we have the opposite situation, whereas for $M_* < M < M_1$ there exist conically self-similar solutions of both kinds. Recall that for fixed J_z, M is a *decreasing* function of Γ_c, and therefore it appears that as the swirl increases any conically self-similar solutions of the near-axis kind must break up, and instead conically self-similar solutions of the two-cell type may appear. However, this behaviour is very similar to that we observe during vortex breakdown. The relatively good performance of M in Table 3.1 therefore naturally raises the question of whether vortex breakdown in swirling annular jets is a transition from an approximately self-similar near-axis jet to an approximately self-similar annular fan jet. In this section we will try to see if swirling annular jets have some approximately conically self-similar features, and to what extent any such structures can be described by the conically self-similar solutions to the Navier-Stokes equations discussed in the previous chapter.

5.2 On the existence of a region of approximately self-similar flow in combustion chambers

In this section we will look for evidence of conically self-similarity in the numerical results we obtained from Case 1 in Chapter 3. When looking for conical self-similarity, a basic difficulty is that we do not know where the apex of the cone is. Due to axisymmetry it must be on the symmetry axis, but it should be emphasised that there is no *a priori* reason to assume that the downstream position of the apex should be same as that of the inlet. In order to find any apices we first consider the radial (in cylindrical co-ordinates) position of the maximum axial velocity as well as that of the maximum circulation for different axial positions.

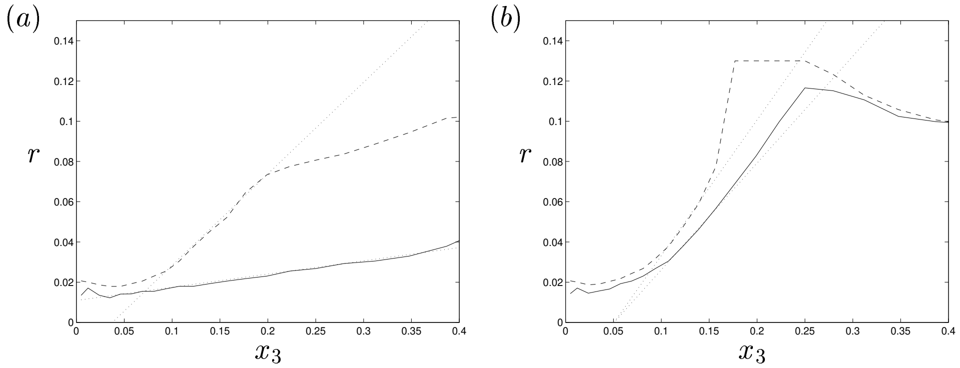

Figure 5.1: The full lines show radial position of maximum circulation, and the dotted lines the maximum axial velocity, as a function of the downstream distance from the orifice, for Case 1 (see Chapter 3) with $Re_z^j = 20300$ and (a) $M^{-\frac{1}{2}} = 0.401$ and (b) $M^{-\frac{1}{2}} = 0.445$. The dotted lines illustrate approximate cones of maximum circulation and axial velocity.

In figure 5.1 (a), which corresponds to a flow just below vortex breakdown, we see that there exists a region where both the circulation and the axial velocity attain their maxima at cones. We also have that the opening angle of the cone of maximum circulation $\theta_c = 24°$ is considerably larger than that of the cone of maximum axial velocity which is only $\theta_s = 4°$. However, the two cones do not have the same apex so the total velocity field is not conically self-similar. However, we can use different apices for the axial velocity and the circulation and rescale them one at a time according to (1.1). The result of such a procedure is shown in figure 5.2, and from this figure we see that between the symmetry axis and the maximum the circulation is approximately conically self-similar, whereas the maximum axial velocity profile becomes increasingly smoothed out as we move downstream.

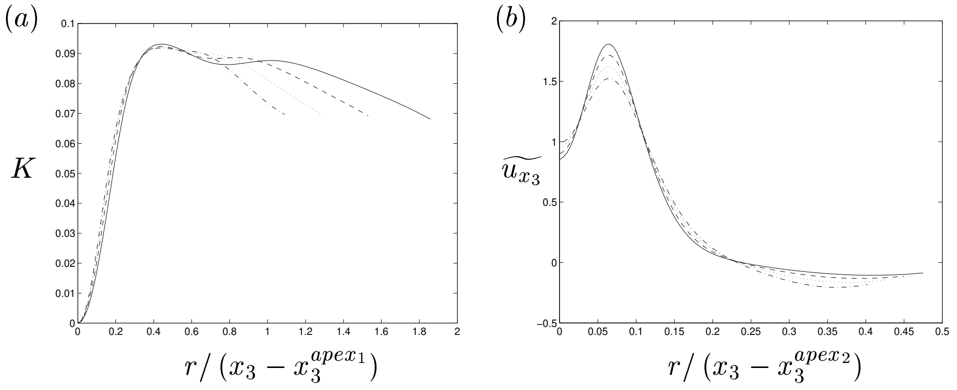

Figure 5.2: The circulation (a) and the axial velocity (b) of Case 1 with $Re_z^j = 20300$ and $M^{-\frac{1}{2}} = 0.401$, as a function of the quotient of the radius and the distance to the apices of their respective cones in figure 5.1(a), at some radial crossections. The solid line corresponds to a radial crossection at $z = 0.1076$, the dashed line to a crossection at $z = 0.1226$, the dotted line to one at $z = 0.1390$ and finally the dashed-dotted line corresponds to a radial crossection at $z = 0.1570$. Here $\widetilde{u_{x_3}} = u_{x_3} \cdot (x_3 - x_3^{apex_2})$, r denotes the cylindrical radius, i.e. the distance to the x_3 axis. Furthermore, $x_3^{apex_1} \approx 0.038$ denotes the apex of the cone of maximum circulation in figure 5.1(a), and $x_3^{apex_2} \approx -0.166$ denotes the apex of the cone of maximum axial velocity in figure 5.1(a).

If we now turn our attention to the same flow case after vortex breakdown, where we have $M^{-\frac{1}{2}} = 0.445$, we find from figure 5.1(b) that there exists a region where the maximal circulation and the maximal axial velocity are approximately attained on cones. This time the cones have a common apex, and similar opening angles: $\theta_c = 34°$ for the circulation and $\theta_s = 28°$ for the axial velocity. Since we have a common apex we can now study degree of conical self-similarity for u_{x_3} and K simultaneously. To enable such a comparison we rescale the velocity components in the spirit of (1.1) and plot them against $\frac{r}{x_3 - x_3^{apex}}$. In figure 5.3, we have done this and here we see that between the symmetry axis and the maxima the flow is approximately conically self-similar when z is between 0.10 and 0.14 approximately. The only major deviation from conical self-similarity in this region occurs for the axial velocity in the central recirculation zone. We also see that it is primarily the amplitude that changes when we begin to leave the region of approximate conical self-similarity. It may seem that region when z is between 0.10 and 0.14 is a very small region, but in fact it is a very important one since most of the development of the central recirculation zone takes place within it.

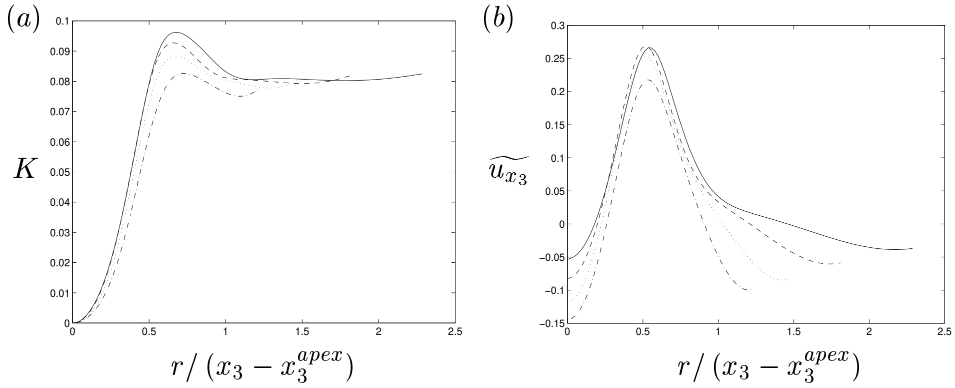

Figure 5.3: The circulation (a) and the axial velocity (b) of Case 1 with $Re_z^j = 20300$ and $M^{-\frac{1}{2}} = 0.445$ as a function of the quotient of the radius and the distance to the common apex of the cones in figure 5.1(b) at radial crossections. The solid line corresponds to a radial crossection at $z = 0.1076$, the dashed line to a crossection at $z = 0.1226$, the dotted line to one at $z = 0.1390$ and finally the dashed-dotted line corresponds to a radial crossection at $z = 0.1570$. Here $\widetilde{u_{x_3}} = u_{x_3} \cdot (x_3 - x_3^{apex})$, r denotes the cylindrical radius, i.e. the distance to the x_3 axis and $x_3^{apex} \approx 0.051$ denotes the common apex of the cones in figure 5.1(b).

We have seen that whereas the fan-jet shows a considerable degree of self-similarity, this is not the case for the near-axis jet. However, we must have in mind that for a near-axis jet there is a strong vortex close to the symmetry axis, and such vortices are known to be poorly treated by the $k - \epsilon$ turbulence model.

5.3 On the relation between the results of CFD simulations of combustion chambers and conically self-similar solutions to the Navier-Stokes equations

5.3.1 Some reasons why combustion chamber flows are *not* conically self-similar

When studying the flow in a combustion chamber, there are several reasons to question the relevance of the conically self-similar solutions discussed in Chapter 4. Firstly, whereas the flow in a combustion chamber is highly turbulent, the conically self-similar solutions to the Navier-Stokes equations are laminar. This, however, is a common problem in jet theory, and for a non-swirling axisymmetric jet it is known, that the basic flow structure remains the same regardless of whether the flow is laminar or turbulent, see [35] and [36]. In [35] it also demonstrated empirically that for non-swirling axisymmetric jet, we may use the laminar velocity profile for the turbulent case as well, as long as we introduce a turbulent viscosity. One may argue that in the case of a swirling conically self-similar solution a similar procedure should be applicable. However, this requires the assumption that the eddy viscosity is approximately constant throughout the flow, and this assumption must, of course, be tested experimentally, and in any case the turbulent viscosity will be a parameter, which we will have to estimate one way or another.

An even more serious difficulty is posed by the geometry. Not only is the downstream position of the apex of the conically self-similar solutions an unknown, which we will have to guess, but the conically self-similar solutions, in fact require an unbounded conical domain. This may be the entire space ($x_c = -1$) a half-space ($x_c = 0$) or any other cone. Furthermore, the conical boundaries are assumed to be streamsurfaces rather than walls. If wall-friction is present, J_z is no longer a conserved quantity and the flow can non longer be conically self-similar. Once again, this is a problem that swirling conically self-similar solutions have in common with non-swirling ones, and for non-swirling jets it is known that for high-Reynolds numbers, the flow remains approximately conically self-similar even though wall-friction is present. We cannot expect a conically self-similar solution to extend itself to a domain where the presence of non-conical boundaries exerts a substantial influence on the fluid, and therefore, for realistic values of $\mathcal{R}$ in figure 1.3, we cannot expect any conically self-similar solution to approximate the flow more than in a fairly small subregion of the total flow domain. Furthermore, the conically self-similar solutions are only far-field solutions to the Navier-Stokes equations, and we cannot expect them to approximate the fluid well in the immediate vicinity of the apex of the cone. Therefore at best we can for a region, which is neither too close to the apex of the cone nor too close to the walls of the combustion chamber. However, if one is going to look for such a region there is yet another problem: What value should we choose for x_c ? There are two situations where the choice is easy. Firstly, if the apex of the cone is far downstream, it seems reasonable to choose $x_c \approx -1$ and if the cone of the apex is very close to the inlet and $r_i \approx 0$ then $x_c = 0$ appears to be a justifiable choice. For other cases, the best solution is perhaps to treat x_c as a free parameter.

5.3.2 The role of Q and L_z in conically self-similar solutions

In Chapter 4 we saw that conically self-similar flows are controlled by the total flow force J_z and the circulation along a streamsurface Γ_c. From (1.1) and the boundary conditions (4.18) and (4.20) it is evident that the mass flow in the cone bounded by $x = 1$ and $x = x_c$ is zero. However, for non-swirling conically self-solutions with $x_c = -1$ it is shown in [17] that we can obtain solutions with arbitrary mass flow by refining (4.2) to

$$u_R = -\frac{\nu\psi'(x)}{R} - \nu\frac{\xi'(x)\ln R + z'(x)}{R^2} \quad \text{and} \tag{5.1}$$

$$u_\theta = -\frac{\nu\psi(x)}{r\sin\theta} - \frac{\nu\xi(x)}{R^2\sin\theta} \,. \tag{5.2}$$

One of the main results in Chapter 4 was that the z-term exists for general x_c, even in swirling case. A necessary condition for a solution like ξ to exist in the swirling case, is that a second order term on the swirl velocity u_ϕ is introduced as well. However, for swirling flow our numerical solutions suggest that the second order non-swirling correction term does allow a net mass flow, which is not the case for non-swirling flow with $x_c = -1$.

The flux of angular momentum L_z, on the other hand, changes linearly with R as is seen from the following calculation:

$$L_z = 2\pi\rho\nu^2 R\int_{x_c}^{1}\left(\psi' - 2\right)\Gamma dx \tag{5.3}$$

$$= -2\pi\rho\nu^2 R\int_{x_c}^{1}\left\{\left(1-x^2\right)\Gamma' - \left(\psi - 2x\right)\Gamma\right\}' dx \tag{5.4}$$

$$= 2\pi\rho\nu^2 R\left[\left(1-x_c^2\right)\Gamma'\left(x_c\right) + 2x_c\Gamma\left(x_c\right)\right] \,. \tag{5.5}$$

Numerical calculations suggest that the quantity inside the brackets is rarely, if ever, zero, and consequently we have a net flux of angular momentum, which was shown by [26]. This change of the flux of angular momentum is due to the torque applied by the streamsurface. To see this we can consider the inviscid case when the linear terms in (4.15) and in (5.3) disappear. L_z would then equal $\psi(-1)\Gamma(-1) - \psi(1)\Gamma(1)$, which clearly is zero. This requirement that angular momentum constantly has to be fed into or drained out of the flow, is obviously another limitation to the spatial duration of conically similar flows. Nevertheless, within a limited region the surrounding fluid may well feed the conical vortex with enough angular momentum (or alternatively drain enough angular momentum out of it) to sustain conical similarity.

If we on the other hand, construct a solution where each of the velocity components are conically self-similar, (which is a weaker requirement than that the entire velocity field is conically self-similar) and require that L_z is kept constant, it is known that the angular velocity will decay as $O\left(R^{-2}\right)$ [19], and it is also known that such solutions do not undergo vortex breakdown.

To summarise, we have found that whereas conservation of J_z and Γ_c along a streamsurface is connected with velocity components decaying as

$O\left(R^{-1}\right)$, the conservation of Q and L_z is connected with velocity components decaying as $O\left(R^{-2}\right)$ or as $O\left(R^{-2}\ln R\right)$. As a consequence, we find that the parameters β and S are both highly unsuitable to describe conically self-similar solutions, since both of them will change as we move away from the apex of the cone.

5.3.3 A numerical comparison

In figure 5.3 we saw some indications that a region of approximate self-similarity may exist in combustion chamber flows. We will now try to get some idea of how well the conically self-similar profiles in figure 5.3 resemble those of the conically self-similar solutions. In this case it is clear that the apex of the cone should be at $x_3^{apex} \approx 0.051$, but to make a comprehensive comparison we would have to estimate a number of parameters like ν the turbulent viscosity, x_c, x_s as well as the value of $z^{'}(1)$, which determines the relative magnitude of the second order swirl-free correction term. In this study, we opted to try only a very limited set of different parameter values. In fact, for x_c we tried only 0 and -1, for x_s we tried some values, the best of which was 0.92 and for ν and $z^{'}(1)$ a limited selection of values were attempted. The result of this comparison is shown in figure 5.4 (with $x_c = -1$) and in figure 5.5 (with $x_c = 0$). Both these figures show a reasonable resemblance between the conically self-similar solution and the numerically obtained CFD solution. Already in figure 5.3 we saw that the axial velocity was not conically self-similar in the central recirculation zone, and therefore it comes as no surprise to us that the velocity profiles are poorly approximated by the conically self-similar solutions in this region. We also see that there is significant deviation close to the combustion chamber wall at $r = 0.13$, but since the conically self-similar solutions do not take any outer walls into account, this discrepancy is expected.

A more interesting feature of the numerical solution, that is not present in the conically self-similar solutions, is the radial peak of the circulation. Intriguingly, this kind of peak is not modelled by the empirically found swirl velocity profile for swirling channel flow, discussed for example in [2]:

$$K = K_\infty\left(1 - e^{-\frac{r^2}{\delta^2}}\right) + \pi\omega r^2 \ , \tag{5.6}$$

where δ and ω are empirical constants. With $\omega = 0$, which is the natural choice when no walls are present, this profile closely resemble those of the conically self-similar solutions. We are thus a position where we do not know whether these peaks really exist, or if they are just the result of numerical error in our CFD calculations.

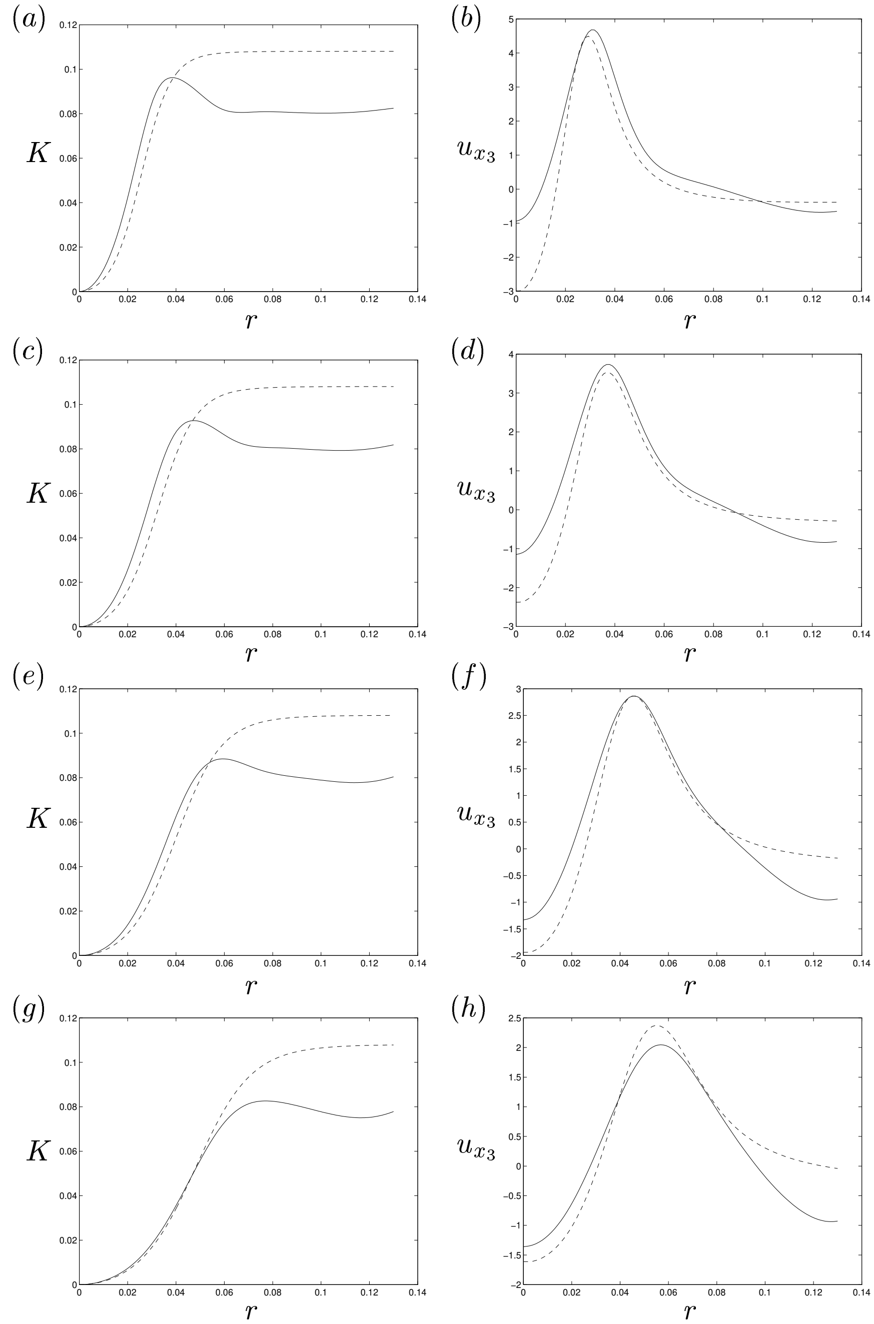

Figure 5.4: The radial profiles of the circulation (a),(c),(e) and (g) and the axial velocity (b),(d),(f) and (h) at several downstream positions. The solid lines come from the CFD calculations of Case 1 (see Chapter 3)with $Re_z^j = 20300$ and $M^{-\frac{1}{2}} = 0.445$, and the dashed lines are conically self-similar solutions with the apex at $x_3 = 0.051$, $\nu = 0.047$, $x_c = -1$, $x_s = 0.92$ and $z^{'}(1) = 0.05$. The radial crossection is taken at $x_3 = 0.1076$ for (a) and (b), at $x_3 = 0.1226$ for (c) and (d), at $x_3 = 0.1390$ for (e) and (f) and at $x_3 = 0.1570$ for (g) and (h).

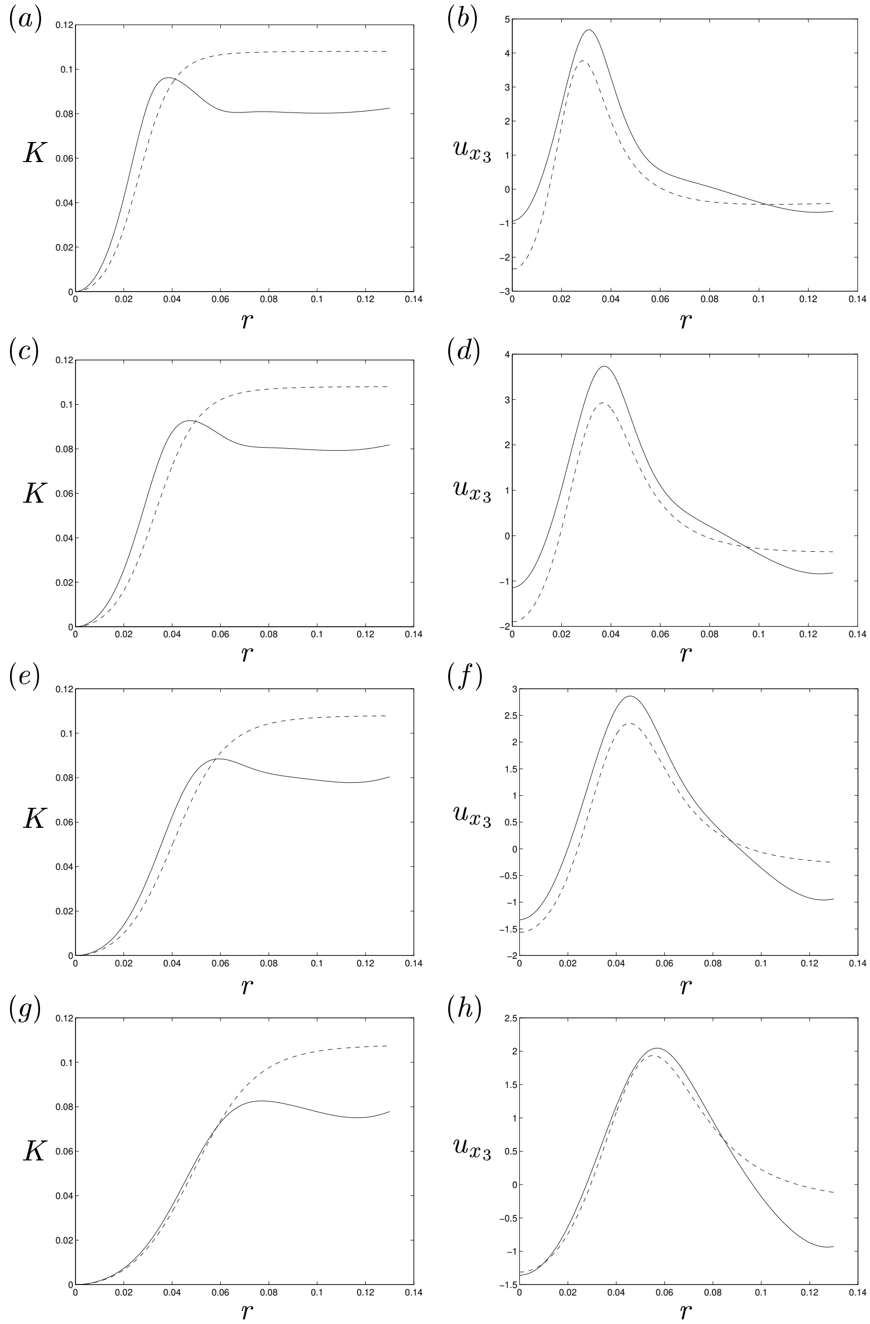

Figure 5.5: The radial profiles of the circulation (a),(c),(e) and (g) and the axial velocity (b),(d),(f) and (h) at several downstream positions. The solid lines come from the CFD calculations of Case 1 (see Chapter 3)with $Re_z^j = 20300$ and $M^{-\frac{1}{2}} = 0.445$, and the dashed lines are conically self-similar solutions with the apex at $x_3 = 0.051$, $\nu = 0.047$, $x_c = 0$, $x_s = 0.92$ and $z^{'}(1) = 0.15$. The radial crossection is taken at $x_3 = 0.1076$ for (a) and (b), at $x_3 = 0.1226$ for (c) and (d), at $x_3 = 0.1390$ for (e) and (f) and at $x_3 = 0.1570$ for (g) and (h).

5.4 On the presence of approximate conical self-similarity in swirling free jets

One of the main reasons why swirling jets in combustion chambers are not conically self-similar is the presence of the outer walls, and therefore it may be that a swirling free jet is better approximated by conically self-similar solutions. Unfortunately, there are, due to the obvious difficulties with the unbounded domain few, if any, numerical simulations of swirling free jets. However, it is a problem examined empirically. Specifically, we have been able to obtain the results of Holzäpfel [37]. In this study an annular inlet with inner radius 26 mm and outer radius 53.5 mm was used. Two different degrees of swirl were considered, and for each of these cases one could find two cones with a common apex such that, within some region, one approximated the position of the maximaum axial velocity and that the other approximated the position of the maximum circulation. We then rescaled the velocity and the circulation according to (1.1) to obtain the profiles shown in figures 5.6 and 5.7.

In the case presented in figure 5.6, we obtain a profile which resembles the conically self-similar near-axis jet solution obtained in figure 4.6(a) and (c). Unfortunately, the Reynolds number of the swirling free jet (which was not given in [37]) seems to be much higher than any our numerical method for calculating conically self-similar solutions can handle. It is also worthwhile to notice the difference in the degree of conical self-similarity for the near axis jets in the experimental measurements of a swirling free jet in figure 5.6 and in the numerical simulation of a combustion chamber flow in 5.2. This difference seems to confirm our suspicion that the $k - \epsilon$ turbulence model does not work very well in the presence of strong near-axis jets. In figure 5.7, the degree of swirl has been increased considerably and the profiles look rather similar to those in figure 5.3.

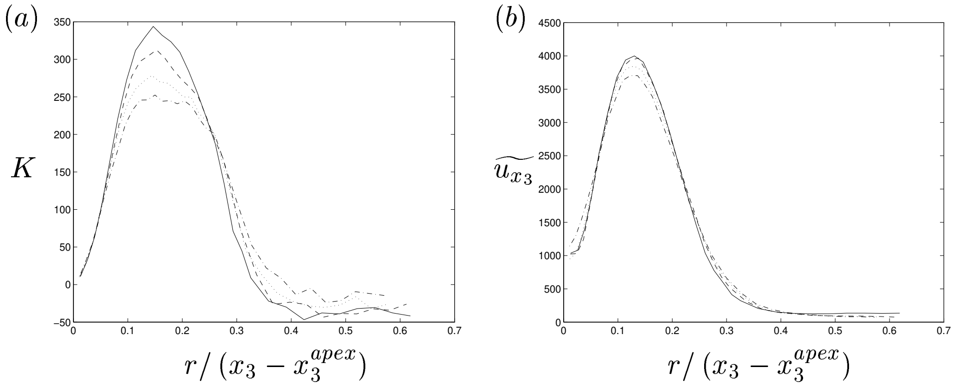

Figure 5.6: The circulation (a) and the axial velocity (b) for a swirling free jet with $S = 0.40$ (see Chapter 3) as a function of the quotient of the radius and the distance to the common apex of the cones of maximum circulation and maximum axial velocity. The results were obtained experimentaly by Holzäpfel [37]. The solid line corresponds to a radial crossection at $z = 0.100$ m, the dashed line to a crossection at $z = 0.120$ m, the dotted line to one at $z = 0.140$ m and finally the dashed-dotted line corresponds to a radial crossection at $z = 0.160$ m. Here $\widetilde{u_{x_3}} = u_{x_3} \cdot (x_3 - x_3^{apex_2})$, r denotes the cylindrical radius, i.e. the distance to the x_3 axis. Furthermore, $x_3^{apex} \approx -0.207$ m denotes the common apex of the cones of maximum circulation and maximum axial velocity.

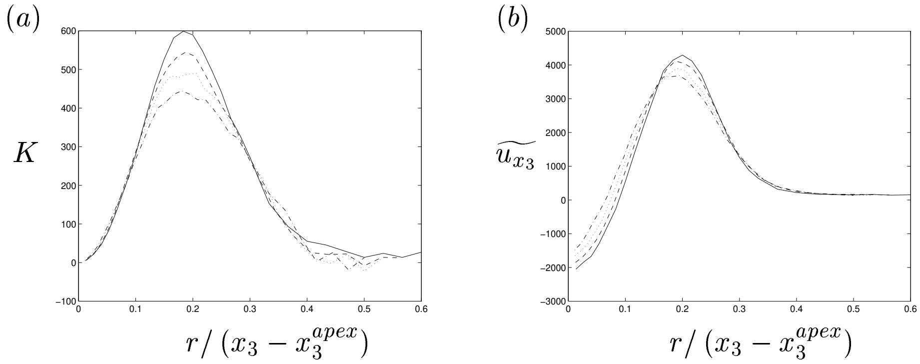

Figure 5.7: The circulation (a) and the axial velocity (b) for a swirling free jet with $S = 0.95$ (see Chapter 3) as a function of the quotient of the radius and the distance to the common apex of the cones of maximum circulation and maximum axial velocity. The results were obtained experimentaly by Holzäpfel [37]. The solid line corresponds to a radial crossection at $z = 0.100$ m, the dashed line to a crossection at $z = 0.120$ m, the dotted line to one at $z = 0.140$ m and finally the dashed-dotted line corresponds to a radial crossection at $z = 0.160$ m. Here $\widetilde{u_{x_3}} = u_{x_3} \cdot (x_3 - x_3^{apex_2})$, r denotes the cylindrical radius, i.e. the distance to the x_3 axis. Furthermore, $x_3^{apex} \approx -0.207$ m denotes the common apex of the cones of maximum circulation and maximum axial velocity.

Chapter 6

Summary

To conclude this report, we briefly recapitulate and comment on our main results.

Our primary concern has been conically self-similar solutions, *i.e.* a class of swirling axisymmetric solutions to the Navier-Stokes equations. We have shown that every conically self-similar solution is analytic in a neighbourhood of its domain. Furthermore we have seen that every conically self-similar solution is uniquely determined by its behaviour on the symmetry axis.

Using these properties we have shown that for every conically self-similar solution there exists a second order non-swirling correction term. In addition, we proved a result, which shows how a second order non-swirling correction term affects the total flux of axial momentum, and we thereby proved an old claim of Burggraf and Foster's [28].

We have also seen that CFD calculations indicate that, for swirling annular jets in cylindrical chambers, there may be a region of approximate conical self-similarity and we have also found some resemblance between the numerical profiles and the conically self-similar solutions. We have also estimated the critical degree of swirl needed for vortex breakdown in CFD calculations, measured in various parameters, for different inlet geometries. In this study the parameter, normally used to formulate vortex breakdown criteria in the theory of conically self-similar solutions, was the parameter, which was the least affected by changes in the inlet geometry.

Notwithstanding that the actual appearance of conically self-similar solutions in real flows is still an open question, this report shows that the class conically self-similar solutions exhibit several qualities typical for swirling flow in general. Therefore it seems likely that an understanding of the properties of conically self-similar solutions will increase the grasp of more general swirling flows.

Appendix A

The incompressible Navier-Stokes equations in spherical co-ordinates

In spherical co-ordinates the continuity equation for an incompressible fluid is given by:

$$\frac{1}{r^2}\frac{\partial}{\partial r}\left(r^2 u_r\right) + \frac{1}{r\sin\theta}\frac{\partial}{\partial\theta}\left(u_\theta \sin\theta\right) + \frac{1}{r\sin\theta}\frac{\partial u_\phi}{\partial\phi} = 0\ . \tag{A.1}$$

The stationary incompressible Navier-Stokes equations are given by:

$$\begin{aligned}
u_r\frac{\partial u_r}{\partial r} + \frac{u_\theta}{r}\frac{\partial u_r}{\partial\theta} + \frac{u_\phi}{r\sin\theta}\frac{\partial u_r}{\partial\phi} - \frac{u_\theta^2 + u_\phi^2}{r} &= -\frac{1}{\rho}\frac{\partial p}{\partial r} + \\
+ \quad \nu\left[\frac{\partial}{\partial r}\left(\frac{1}{r^2}\frac{\partial}{\partial r}\left(r^2 u_r\right)\right) + \frac{1}{r^2\sin\theta}\frac{\partial}{\partial\theta}\left(\sin\theta\frac{\partial u_r}{\partial\theta}\right) + \right. \\
+ \quad \left. \frac{1}{r^2\sin^2\theta}\frac{\partial^2 u_r}{\partial\phi^2} - \frac{2}{r^2\sin\theta}\frac{\partial}{\partial\theta}\left(u_\theta\sin\theta\right) - \frac{2}{r^2\sin\theta}\frac{\partial u_\phi}{\partial\phi}\right]
\end{aligned} \tag{A.2}$$

$$\begin{aligned}
\frac{u_r}{r}\frac{\partial}{\partial r}\left(r u_\theta\right) + \frac{u_\theta}{r}\frac{\partial u_\theta}{\partial\theta} + \frac{u_\phi}{r\sin\theta}\frac{\partial u_\theta}{\partial\phi} - \frac{u_\phi^2\cot\theta}{r} &= -\frac{1}{\rho r}\frac{\partial p}{\partial\theta} + \\
+ \quad \nu\left[\frac{1}{r^2}\frac{\partial}{\partial r}\left(r^2\frac{\partial u_\theta}{\partial r}\right) + \frac{1}{r^2}\frac{\partial}{\partial\theta}\left(\frac{1}{\sin\theta}\frac{\partial}{\partial\theta}\left(u_\theta\sin\theta\right)\right) + \right. \\
+ \quad \left. \frac{1}{r^2\sin^2\theta}\frac{\partial^2 u_\theta}{\partial\phi^2} + \frac{2}{r^2}\frac{\partial u_r}{\partial\theta} - \frac{2\cot\theta}{r^2\sin\theta}\frac{\partial u_\phi}{\partial\phi}\right]
\end{aligned} \tag{A.3}$$

$$\begin{aligned}
\frac{u_r}{r}\frac{\partial}{\partial r}\left(r u_\phi\right) + \frac{u_\theta}{r}\frac{\partial u_\phi}{\partial\theta} + \frac{u_\phi}{r\sin\theta}\frac{\partial u_\phi}{\partial\phi} + \frac{u_\theta u_\phi}{r}\cot\theta &= -\frac{1}{\rho r\sin\theta}\frac{\partial p}{\partial\phi} + \\
+ \quad \nu\left[\frac{1}{r^2}\frac{\partial}{\partial r}\left(r^2\frac{\partial u_\phi}{\partial r}\right) + \frac{1}{r^2}\frac{\partial}{\partial\theta}\left(\frac{1}{\sin\theta}\frac{\partial}{\partial\theta}\left(u_\phi\sin\theta\right)\right) + \right. \\
+ \quad \left. \frac{1}{r^2\sin^2\theta}\frac{\partial^2 u_\phi}{\partial\phi^2} + \frac{2}{r^2\sin\theta}\frac{\partial u_r}{\partial\phi} + \frac{2\cot\theta}{r^2\sin\theta}\frac{\partial u_\theta}{\partial\phi}\right]
\end{aligned} \tag{A.4}$$

Bibliography

[1] T. B. Benjamin, "Theory of the vortex breakdown phenomenon," *Journal of Fluid Mechanics*, vol. 14, pp. 593–629, 1962.

[2] M. Escudier, "Vortex breakdown: Observations and explanations," *Progress in Aerospace Science*, vol. 25, pp. 189–229, 1988.

[3] R. L. Panton, *Incompressible Flow.* New York: John Wiley & Sons, 1984.

[4] R. R. Long, "Vortex motion in a viscous fluid," *Journal of Meteorology*, vol. 15, pp. 108–112, 1958.

[5] V. Shtern and F. Hussain, "Hysteresis in swirling jets," *Journal of Fluid Mechanics*, vol. 309, pp. 1–44, 1996.

[6] L. E. Eriksson, "Development and validation of highly modular flow solver versions in g2dflow and g3dflow series for compressible viscous reacting flow," Report 9970-1162, Volvo Aero Corporation, 1995.

[7] J. Larsson, "Numerical simulation of turbine blade heat transfer," Thesis for the Degree of Licenciate of Engineering 96/4, Chalmers University of Technology, 1996.

[8] H. J. Sheen, W. J. Chen, and S. Y. Jeng, "Recirculation zones of unconfined and confined annular swirling jets," *AIAA Journal*, vol. 34, no. 3, pp. 572–580, 1996.

[9] M. P. Escudier and J. J. Keller, "Recirculation in swirling flow: A manifestation of vortex breakdown," *AIAA Journal*, vol. 23, no. 1, pp. 111–116, 1985.

[10] H. Schlichting, "Laminaire strahlausbreitung," *Zeitschrift für Angewandte Mathematik und Mechanik*, vol. 13, pp. 260–263, 1933.

[11] L. D. Landau, "On a new exact solution of the Navier-Stokes equations," *Dokl. Akad. Nauk SSSR*, vol. 43, pp. 299–301, 1944.

[12] J. K. Harvey, "Some observations of the vortex breakdown phenomenon," *Journal of Fluid Mechanics*, vol. 14, pp. 585–592, 1962.

[13] T. Sarpkaya, "Vortex breakdown in swirling conical flows," *AIAA Journal*, vol. 9, no. 9, pp. 1792–1799, 1971.

[14] Y. L. Lai, "Predictive capabilities of turbulence models for a confined swirling flow," *AIAA Journal*, vol. 34, no. 8, pp. 1743–1745, 1996.

[15] L. G. Loitsyanskii, "Propagation of a swirling jet in unbounded space filled with the same fluid," *Prikl. Matem. Mekhan.*, vol. 17, pp. 3–16, 1953.

[16] M. A. Goldshtik, "On swirling jets," *Fluid Dynamics*, vol. 14, pp. 19–26, 1979.

[17] M. A. Goldshtik and N. I. Yavorskii, "On submerged jets," *Prikl. Matem. Mekhan.*, vol. 50, no. 4, pp. 438–445, 1986.

[18] H. Görtler, "Decay of swirl in an axially symmetrical jet, far from the orifice," *Revista Matematica Hispano-America IV*, vol. 14, pp. 143–178, 1954.

[19] M. S. Tsukker, "A swirling jet propagating in a space filled with the same fluid," *Prikl. Matem. Mekhan.*, vol. 19, pp. 500–503, 1955.

[20] R. R. Long, "A vortex in an infinate viscous fluid," *Journal of Fluid Mechanics*, vol. 11, pp. 611–624, 1961.

[21] M. A. Goldshtik, "A paradoxical solution of the Navier-Stokes equations," *Prikl. Matem. Mekhan.*, vol. 24, pp. 610–621, 1960.

[22] J. Serrin, "The swirling vortex," *Philosophical Transactions of the Royal Society of London Ser. A*, vol. 271, pp. 325–360, 1972.

[23] M. A. Goldshtik, "Viscous-flow paradoxes," *Annular Review of Fluid Dynamics*, vol. 22, pp. 441–472, 1990.

[24] C.-S. Yih, F. Wu, A. K. Garg, and S. Leibovich, "Conical vortices: A class of exact solutions of the Navier-Stokes equations," *The Physics of Fluids*, vol. 25, no. 12, pp. 2147–2158, 1982.

[25] M. A. Goldshtik and V. N. Shtern, "Collapse in viscous flows," *Journal of Fluid Mechanics*, vol. 218, pp. 483–508, 1989.

[26] R. Paull and A. F. Pillow, "Conically similar viscous flows. Part 3. Characterization of axial causes in swirling flow and the one-parameter flow generated by a uniform half-line source of kinematic swirl angular momentum," *Journal of Fluid Mechanics*, vol. 155, pp. 359–379, 1985.

[27] V. Shtern and F. Hussain, "Hysteresis in a swirling jet as a model tornado," *The Physics of Fluids A*, vol. 5, no. 9, pp. 2183–2195, 1993.

[28] O. R. Berggraf and M. R. Foster, "Continuation or breakdown in tornado-like vortices," *Journal of Fluid Mechanics*, vol. 80, pp. 685–703, 1977.

[29] P. G. Drazin, W. H. H. Banks, and M. B. Zaturska, "The development of long's vortex," *Journal of Fluid Mechanics*, vol. 286, pp. 359–377, 1995.

[30] C. Sozou, "On solutions relating to conical vortices over a plane wall," *Journal of Fluid Mechanics*, vol. 244, pp. 633–644, 1992.

[31] P. Painlevé, *Leçons sur la théorie analytique des équations différentielles, professées à Stockholm.* 1897.

[32] E. L. Ince, *Ordinary Differential Equations.* New York: Dover Publications Inc, 1956.

[33] K. G. Andersson and L. C. Böiers, *Ordinära differentialekvationer.* Lund: Studentlitteratur, 1989. (in Swedish).

[34] G. Birkhoff and G. C. Rota, *Ordinary Differential Equations.* Boston: Ginn and Company, 1962.

[35] H. Schlichting, *Boundary - Layer Theory.* New York: McGraw - Hill Book Company, 1979.

[36] H. Tennekes and J. L. Lumley, *A First Course in Turbulence.* Cambridge (Mass): MIT Press, 1972.

[37] F. Holzäpfel, *Zur Turbulenzstruktur freier und eingeschlossener Drehströmungen.* PhD thesis, Universität Fridericiana Karlsruhe (Technische Hochschule), 1996.